OAK RIDGE NATIONAL LABORATORY LIBRARIES
3 4456 0566314 5

ornl

ORNL/TM-11162

OAK RIDGE NATIONAL LABORATORY

MARTIN MARIETTA

# Selection of Corrosion-Resistant Materials for Use in Molten Nitrate Salts

P. F. Tortorelli
P. S. Bishop
J. R. DiStefano

OPERATED BY
MARTIN MARIETTA ENERGY SYSTEMS, INC.
FOR THE UNITED STATES
DEPARTMENT OF ENERGY

This report has been reproduced directly from the best available copy.

Available to DOE and DOE contractors from the Office of Scientific and Technical Information, P.O. Box 62, Oak Ridge, TN 37831; prices available from (615) 576-8401, FTS 626-8401.

Available to the public from the National Technical Information Service, U.S. Department of Commerce, 5285 Port Royal Rd., Springfield, VA 22161.
NTIS price codes—Printed Copy: A04 Microfiche A01

This report was prepared as an account of work sponsored by an agency of the United States Government. Neither the United States Government nor any agency thereof, nor any of their employees, makes any warranty, express or implied, or assumes any legal liability or responsibility for the accuracy, completeness, or usefulness of any information, apparatus, product, or process disclosed, or represents that its use would not infringe privately owned rights. Reference herein to any specific commercial product, process, or service by trade name, trademark, manufacturer, or otherwise, does not necessarily constitute or imply its endorsement, recommendation, or favoring by the United States Government or any agency thereof. The views and opinions of authors expressed herein do not necessarily state or reflect those of the United States Government or any agency thereof.

ORNL/TM-11162

Metals and Ceramics Division

# SELECTION OF CORROSION RESISTANT MATERIALS FOR USE IN MOLTEN NITRATE SALTS

P. F. Tortorelli, P. S. Bishop, and J. R. DiStefano

Date Published: October 1989

NOTICE: This document contains information of a preliminary nature. It is subject to revision or correction and therefore does not represent a final report.

Prepared for the DOE
Assistant Secretary for Conservation and Renewable Energy
Office of Industrial Programs
Waste Energy Recovery Program
ED 02 11 00 0

and

Office of Energy Utilization Research
Energy Conversion and Utilization Technologies Program
EG 05 03 00 0

Prepared by the
Oak Ridge National Laboratory
Oak Ridge, Tennessee 37831-6285
operated by
MARTIN MARIETTA ENERGY SYSTEMS, INC.
for the
U.S. DEPARTMENT OF ENERGY
under contract DE-AC05-84OR21400

CONTENTS


| | Page |
|---|---|
| LIST OF FIGURES | v |
| LIST OF TABLES | ix |
| ABSTRACT | 1 |
| INTRODUCTION | 1 |
| EXPERIMENTAL PROCEDURES | 3 |
| EQUIPMENT DESCRIPTION | 3 |
| SALT COMPOSITIONS | 6 |
| SPECIMEN PREPARATION | 7 |
| RESULTS | 9 |
| WEIGHT CHANGE MEASUREMENTS | 9 |
| MICROSTRUCTURAL ANALYSES | 18 |
| DISCUSSION | 29 |
| SUMMARY | 45 |
| REFERENCES | 47 |

LIST OF FIGURES


| Figure | | Page |
|---|---|---|
| 1 | Schematic drawing of sparged molten nitrate salt crucible assembly | 4 |
| 2 | Schematic drawing of sparged molten nitrate salt exposure system | 5 |
| 3 | Average weight change for different materials exposed to $NaNO_3$-$KNO_3$-$Na_2O_2$ at 650°C for ~24 h | 12 |
| 4 | Average weight change for iron aluminides exposed to $NaNO_3$-$KNO_3$ (Na,K) or $NaNO_3$ (Na) at 650°C for ~24 h (Al concentrations in at. %) | 13 |
| 5 | Weight loss vs exposure time for $NaNO_3$-$KNO_3$(-$Na_2O_2$) at 650°C. (*a*) Fe-35 at. % Al, (*b*) NiAl | 14 |
| 6 | Average weight change for Fe-35 at. % Al exposed to $NaNO_3$-$KNO_3$-$Na_2O_2$ (Na,K) or $NaNO_3$ (Na) at 650°C for ~24 h | 15 |
| 7 | Cumulative weight losses vs time for Fe-35 at. % Al exposed to (Na,K)$NO_3$(-1 mol % $Na_2O_2$) at 661°C for salt conditions B (peroxide added at start of exposure interval) and C (no new peroxide added) | 16 |
| 8 | Cumulative weight losses vs time for Fe-35 at. % Al exposed to $NaNO_3$-$KNO_3$-1% $Na_2O_2$ at 661 and 684°C. Peroxide was refreshed during each exposure segment | 16 |
| 9 | Average weight change as a function of aluminum concentration for iron aluminides exposed to $NaNO_3$-$KNO_3$-$Na_2O_2$ or $NaNO_3$-$Na_2O_2$ at 650°C for 20 to 30 h | 17 |
| 10 | Average weight losses of $Ni_3Al$ and NiAl exposed to $NaNO_3$-$KNO_3$-$Na_2O_2$ at 650°C for ~24 h | 18 |
| 11 | Weight losses of $Ni_3Al$ and NiAl exposed to $NaNO_3$-$KNO_3$-$Na_2O_2$ at 650°C for ~24 h. Uncoated data represent averages; values for coated specimens are for individual specimens with yttrium-stabilized zirconate coatings deposited by plasma spraying | 19 |
| 12 | Polished cross sections of specimens exposed for about 48 h to static $NaNO_3$-$KNO_3$-$Na_2O_2$ at 650°C at APCI; (*a*) Ni-200, 99.0 Ni, 0.075 C, 0.0007 S (wt %); (*b*) Ni-270, 99.97 Ni, 0.02 C, 0.0013 S; (*c*) high purity Ni, 99.9975 Ni, 0.0073 C, 0.0019 S | 20 |

| Figure | | Page |
|---|---|---|
| 13 | Polished cross sections of $Ni_3Al$ exposed for about 48 h to static $NaNO_3$-$KNO_3$-$Na_2O_2$ at 650°C at APCI; (*a*) as-wrought; (*b*) preoxidized | 22 |
| 14 | Polished cross section of alloy 600 exposed to $NaNO_3$-$KNO_3$-$Na_2O_2$ for 24 h at 650°C | 23 |
| 15 | Polished cross section of alloy 600 exposed in MOLTOX pilot plant at 650°C | 23 |
| 16 | Polished cross section of alloy 800 exposed in MOLTOX pilot plant at 650°C | 23 |
| 17 | Schematic drawing of heavily aluminized Fe-Ni-Cr or Ni-Cr-Fe alloy based on microstructural analysis of unexposed aluminized alloy 800 and type 316 stainless steel | 25 |
| 18 | Polished cross section of aluminized alloy 800 exposed in MOLTOX pilot plant at 650°C | 25 |
| 19 | Elemental X-ray maps from polished cross section of aluminized alloy 800 exposed in MOLTOX pilot plant at 650°C | 26 |
| 20 | Polished cross section of aluminized type 316 stainless steel exposed in MOLTOX pilot plant at 510°C | 27 |
| 21 | Polished cross section of Fe-35 at. % Al exposed to $NaNO_3$-$KNO_3$-$Na_2O_2$ for 24 h at 650°C | 28 |
| 22 | Polished cross section of zirconium exposed to $NaNO_3$-$KNO_3$-$Na_2O_2$ for 23.5 h at 650°C | 30 |
| 23 | Polished cross section of zirconium exposed to $NaNO_3$-$KNO_3$-$Na_2O_2$ in air for 24 h at 650°C | 31 |
| 24 | Measured weight gains vs total layer thickness for zirconium exposed to nitrate salt in air at 650°C | 32 |
| 25 | Polished cross section of zirconium exposed to $NaNO_3$-$KNO_3$-$Na_2O_2$ in air at 650°C; (*a*) 96 h, (*b*) 305 h, (*c*) 760 h | 33 |
| 26 | Square of layer thickness vs exposure time for zirconium exposed to nitrate salt in air at 650°C | 34 |
| 27 | Polished cross sections of hafnium exposed to $NaNO_3$-$KNO_3$-$Na_2O_2$ at 650°C; (*a*) 24 h, (*b*) 39.6 h | 35 |

| Figure | | Page |
|---|---|---|
| 28 | Phase stability diagram of the Fe-Na-K-N-O-Ar system at 677 and 507°C. The ratio of Na:K:Fe is 50:50:0.01 . . | 37 |
| 29 | Phase stability diagram of the Al-Na-K-N-O-Ar system at 677 and 507°C. The ratio of Na:K:Al is 50:50:0.01 . . | 38 |

LIST OF TABLES


| Table | | Page |
|---|---|---|
| 1 | Materials exposed in ORNL's sparged molten salt exposure system | 8 |
| 2 | Weight changes of pure metals exposed to nitrate salt at 650°C for ~24 h | 9 |
| 3 | Weight changes of alloys exposed to molten nitrate salt at 650°C for ~24 h | 10 |
| 4 | Weight changes of bulk ceramics exposed to nitrate salt at 650°C for ~24 h | 11 |
| 5 | Ratio of chromium concentration in thin surface layer to bulk chromium concentration for alloys exposed to $(Na,K)NO_3$-$Na_2O_2$ at 650°C | 24 |

# SELECTION OF CORROSION-RESISTANT MATERIALS FOR USE IN MOLTEN NITRATE SALTS*

P. F. Tortorelli, P. S. Bishop, and J. R. DiStefano

## ABSTRACT

Investigations of the corrosion of various metals, alloys, and ceramics in high-temperature nitrate salt melts revealed that relatively few materials have acceptable compatibility in a 650°C, $NaNO_3$(-$KNO_3$)-$Na_2O_2$ environment that was chemically characteristic of the MOLTOX™ chemical air separation process. Corrosion in these systems was controlled by the stabilities of the salt and solid-state surface oxides (whether they were pre-existing or formed upon exposure), the salt's oxide ion activity (strongly influenced by $Na_2O_2$ additions), and the physical condition of the solid surfaces. In general, refractory/reactive metals and alloys (with the exception of zirconium and hafnium), cobalt, nickel, NiMo, TiAl, austenitic stainless steel, and Ni-Cr-Fe alloys were found to corrode quite readily because of rapid oxidation and/or dissolution in the salt. $Ni_3Al$ had a more moderate corrosion rate, while NiAl and iron aluminides with greater than about 35 at. % Al performed relatively well. Zirconium formed an apparently adherent corrosion product, but its scaling kinetics were sufficiently high to make long-term exposure to the salt problematical. Hafnium appeared to be the most corrosion-resistant metallic material. High-density $Al_2O_3$, $ZrO_2$, and MgO were quite stable in the salt, but more porous ceramics did not perform well due to salt uptake and mechanical crumbling. A similar degradation phenomenon was observed for plasma-sprayed zirconate coatings on nickel aluminides. Analysis of specimens exposed in the Air Products and Chemicals, Inc., MOLTOX™ pilot plant showed that commercially aluminized coatings on Fe-Ni-Cr and Ni-Cr-Fe alloys did not impart any increased protection to the substrate materials because of extensive cracking of the high aluminum surface layers.

There was some evidence that $NaAlO_2$ formed on aluminum-containing surfaces, and it was determined to be thermodynamically stable in the nitrate salt environment. However, this product was never observed to be adherent to

---

*Research sponsored by the Assistant Secretary for Conservation and Renewable Energy, Office of Industrial Programs and Office of Energy Utilization Research, Energy Conversion and Utilization Technologies (ECUT) Program, U.S. Department of Energy, under contract DE-AC05-84OR21400 with Martin Marietta Energy Systems, Inc.

the exposed material. Nevertheless, the formation of $NaAlO_2$ and a thin $Al_2O_3$ surface layer apparently were the cause of lower reaction rates of iron aluminides compared with most other candidate alloys. The presence of $Na_2O_2$ in the nitrate exacerbated the corrosion of aluminides because of an increase in the basicity of the salt; however, for a fixed concentration, its influence decreased with time. Weight-loss kinetics were approximately linear for Fe-35 at. % Al when the $Na_2O_2$ content of the salt was periodically refreshed (which more closely simulates the MOLTOX™ condition).

---

## INTRODUCTION

The physical properties of molten nitrate salts make them attractive candidates for use as heat transfer and storage media. For example, they are used to remove or provide heat for chemical reactions and as heat treatment baths[1] and can serve as the coolant and thermal energy storage materials for solar power towers.[2] In addition, the chemical properties of nitrate salts can be exploited to produce high-purity oxygen and nitrogen gases at substantial energy savings compared to cryogenic production of oxygen.[3] However, in this MOLTOX* process, the operating temperature and salt composition combine to present a very corrosive environment for typical materials of construction.[3] A study was therefore conducted to more fully characterize the corrosion reactions in molten sodium-potassium nitrate salts appropriate to the MOLTOX process and to define materials that are corrosion resistant in this type of environment. This report summarizes the results and analyses from this effort.

Electrochemical and corrosion studies with molten sodium and sodium-potassium nitrate salts have been previously conducted (see, e.g., refs. 4-16), although none involved the very aggressive environment characteristic of the prototypic salt used in the present case (see below). The greatest recent effort in studying corrosion by molten nitrate salts was that of Bradshaw et al.,[4-8] who examined

---

*Trademark of Air Products and Chemicals, Inc., Allentown, PA.

stainless steels and alloy 800 in thermal convection loops as well as a variety of materials exposed to static salt. These studies showed that, in general, corrosion resistance was acceptable below 600°C, but that above this temperature, extensive oxidation and depletion of chromium (due to the high solubility of the chromate ion in the salt) occurred. Whereas the overall corrosion rate was parabolic up to 600°C, nonprotective corrosion behavior (linear kinetics) was evident above 615°C. Results from less extensive work with stainless steels and alloy 800 in thermal convection loops[9] agreed with the findings of Bradshaw et al. At temperatures between 250 and 500°C, iron,[10-12] mild steel,[13-14] and pure nickel[15] showed passivation characteristics in molten sodium-potassium nitrate salt in agreement with thermodynamic considerations.[10-12,16]

## EXPERIMENTAL PROCEDURES

### EQUIPMENT DESCRIPTION

A cross-sectional view of the crucible assembly used for the exposures of the specimens to the molten nitrate salt is shown in Fig. 1. Continuous sparging of the melt with dry air was maintained during specimen exposures using gas bubbler tubes. The crucibles (30.5 cm long with an outer diameter of 5.7 cm) and bubbler tubes were made of alumina and were replaced after each melt cycle. The tubes were positioned and supported by the compression of an O-ring in one of the three fittings on a stainless steel end flange. This flange was sealed to the crucible using a Viton gasket. A specimen was suspended on the end of a wire (usually 0.5-mm-diam zirconium) in the salt. The other end of the wire was attached to a 6.4-mm-diam nickel rod, which was supported by the compression of an O-ring in another of the end flange fittings. Specimens were normally positioned approximately halfway down into the salt. Gases were vented from the crucible through the third flange fitting.

ORNL-DWG-89-11741

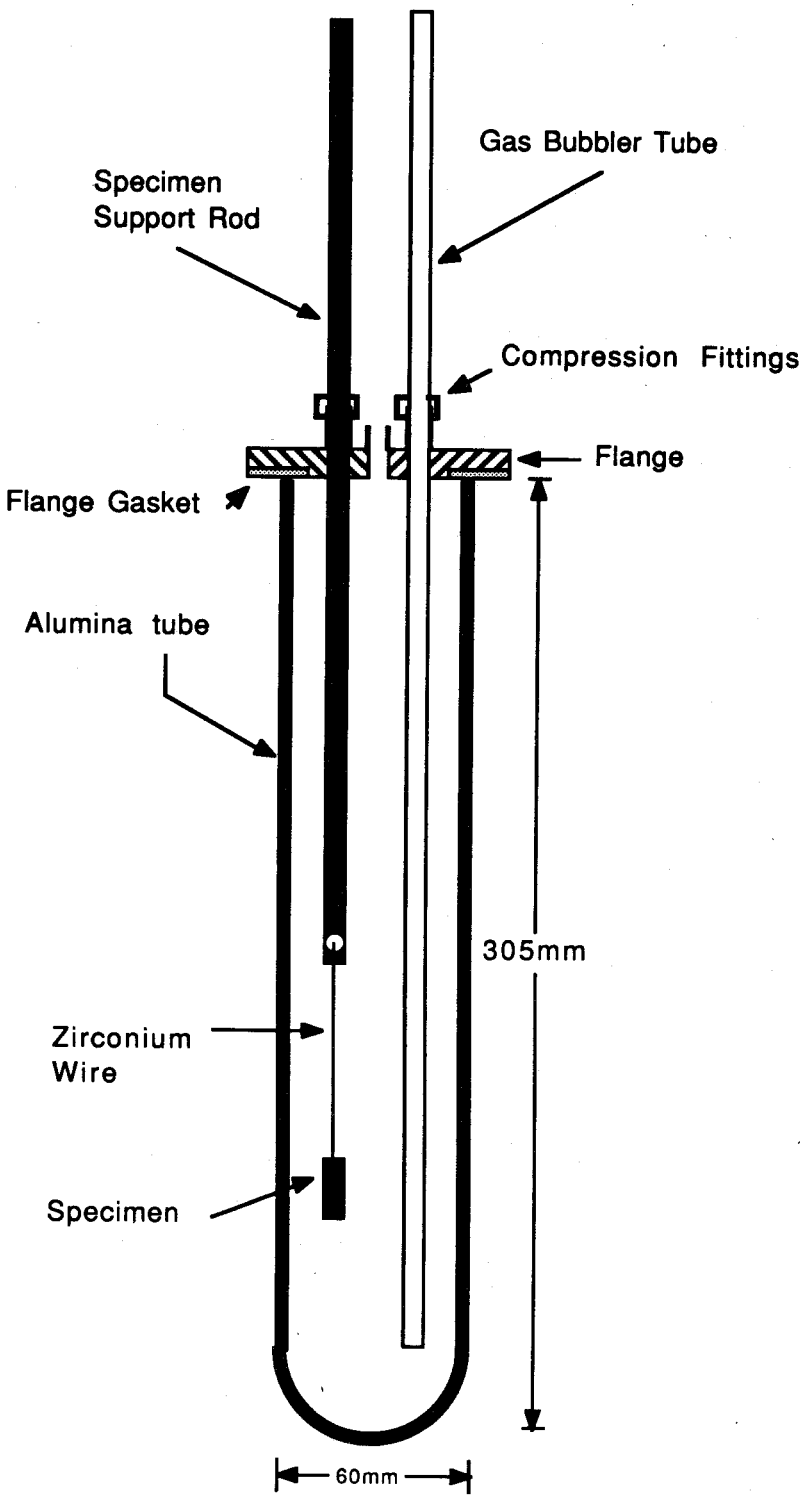


Fig. 1. Schematic drawing of sparged molten nitrate salt crucible assembly.

The cross-sectional schematic drawing (see Fig. 2) shows the entire experimental exposure system. Each crucible sat on sufficient firebrick and insulation to position the Viton gasket 5 cm above the furnace. Insulation was used to center the crucible in the furnace and to surround that part of the crucible above the furnace. Each furnace had an operating range of 25 to 1204°C and was located in an isolation booth equipped to provide exhaust ventilation, thermocouple leads, electrical power, compressed air, water, drains, and connections to an external gas supply. A manifold in the booth delivered regulated breathing air to

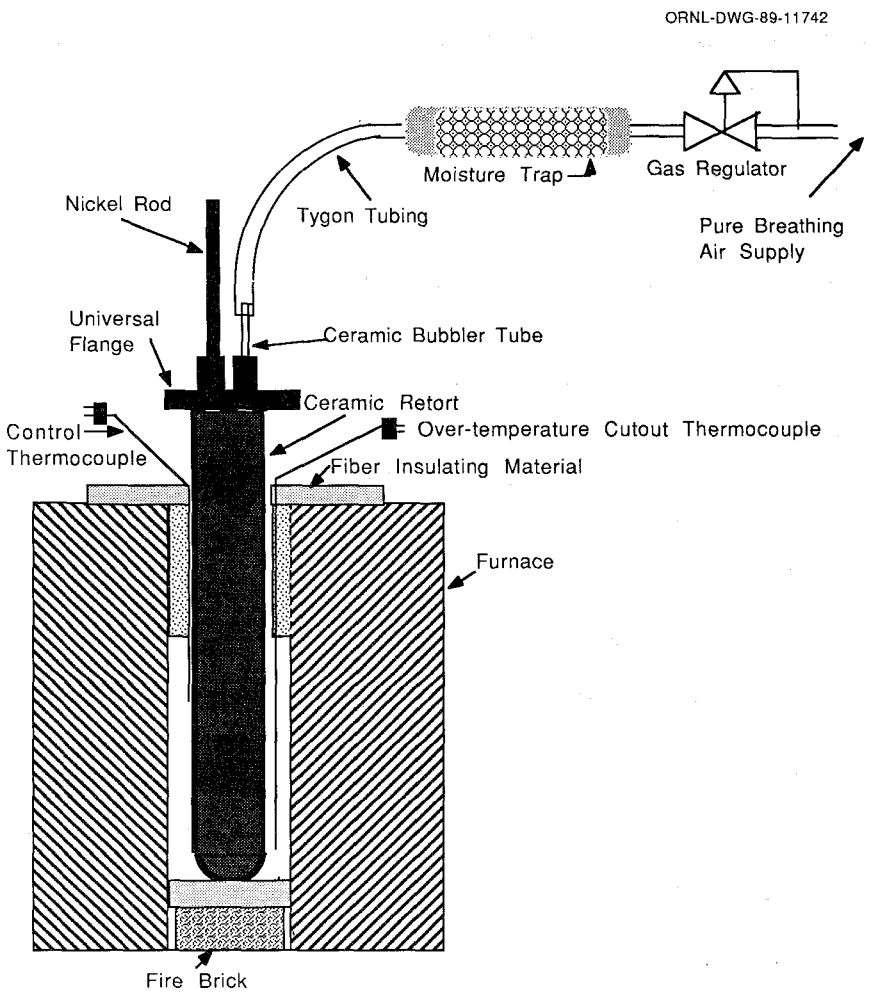


Fig. 2. Schematic drawing of sparged molten nitrate salt exposure system.

the crucible bubbler tube via a moisture trap (containing anhydrous $CaSO_4$) and flowmeter. The typical flow rate of dry air through the bubbler tube was 85 l/h. Two chromel-alumel thermocouples were located between the crucible and the heating surface of the furnace. One thermocouple was located about 13 cm from the bottom of the crucible and provided the signal for controlling the furnace temperature. The other thermocouple was located near the bottom of the crucible and supplied an independent signal for overtemperature protection. The relationship between the output from these thermocouples and the actual melt temperature (measured using a thermocouple inserted into the salt) was established prior to the start of specimen exposures, and the correlation was then checked periodically throughout the time a particular melt was used.

## SALT COMPOSITIONS

Two different nitrate salt compositions were used in the present study. Salt composition 1 contained 49 mol % $NaNO_3$ (44.7% by weight) and 51 mol % $KNO_3$ (55.3% by weight). Additions of 1 mol % $Na_2O_2$ (0.85% by weight) were made to obtain the "B" condition. Composition 2 was 100% $NaNO_3$; 0.4 mol % $Na_2O_2$ (0.4% by weight) was added to obtain the "B" condition. Each salt was in one of three conditions, designated with the letter A, B, or C, as follows:

A: a nitrate salt with no $Na_2O_2$ added.

B: a nitrate salt with $Na_2O_2$ added just prior to or during the exposure of a specific specimen.

C: a salt with $Na_2O_2$ added, but no $Na_2O_2$ added just prior to or during the exposure of a specific specimen.

All of the components used to make the salts were reagent grade. They were weighed on a 0.0 to 311.0-g mechanical balance. To facilitate additions to the molten salt during operation, $Na_2O_2$ was measured into individual containers in an inert atmosphere (to reduce moisture absorption). Single portions were then added to the melt through the crucible vent. The salt was kept molten between specimen exposures and was replaced only periodically.

## SPECIMEN PREPARATION

Prior to exposure, materials selected for exposure were sheared or cut as close as possible to the nominal specimen dimensions, 5.1 × 2.5 × 19 mm. In some cases, a 1.5-mm-diam hole was drilled at one end of the specimen. Rough edges were removed by grinding and sanding. Selected specimens were then annealed. Final preparation involved surface cleaning using solvents compatible with the particular specimen material. All dimensional measurements were made with a dial caliper, and all weights were measured with an electronic balance. A wire (normally zirconium) was inserted through the specimen hole or used to form a basket around the specimen to suspend it in the salt. Upon removal from the salt, all specimens were visually inspected, and any unusual observations were noted. Specimens were allowed to cool in air and were then rinsed in hot water. The wire was removed, and the specimen was again rinsed. After air drying, the specimens were weighed, and their dimensions were recorded. The corroded surfaces and polished cross sections of selected specimens were analyzed by optical and scanning electron microscopy and energy-dispersive X-ray analysis (EDX). In certain cases, the salt adhering to the specimen was not removed after exposure, and special dry polishing techniques were used during the metallographic preparation of a cross section. Table 1 lists the different materials exposed to the molten salt, their compositions, and the number of specimens of each used in the corrosion experiments.

In addition to microstructural analysis of selected ORNL specimens, some materials exposed under prototypic MOLTOX salt conditions at Air Products and Chemicals, Inc. (APCI) were analyzed by scanning electron microscopy and electron-probe microanalysis at ORNL during the initial stage of these investigations. APCI specimens were either coupons similar to those described previously (used for exposures to static salt) or segments of tubes exposed in the MOLTOX pilot plant.[3] Several of these specimens were aluminized prior to the salt exposures by the ALON process.

Table 1. Materials exposed in ORNL's sparged molten salt exposure system

| Material | Laboratory name | Element (%) | | | | | No. of tests |
|---|---|---|---|---|---|---|---|
| | | Al | Cr | Ni | Zr | Other | |
| Cobalt | | | | | | | 2 |
| Iron | | | | | | | 2 |
| Hafnium | | | | | | | 11 |
| Titanium | | | | | | | 2 |
| Zirconium | | | | | | | 30 |
| Nickel | Alloy 600 | | | | | 9.0Fe-0.4Cu-0.2Si | 12 |
| Alumina | Al-08 | | | | | | 5 |
| | Al-35 | | | | | 0.05MgO | 3 |
| | SCW-227[a] | | | | | 0.1MgO, 10 wt % SiC | 2 |
| | SCW-228[a] | | | | | 0.1MgO, 30 wt % SiC | 3 |
| | FG $Al_2O_3$ | | | | | Fine grained, 0.1MgO | 2 |
| | Fe-32Ni-32Al | 19.0 | | 40.0 | | | 4 |
| | Fe-26Al | 14.5 | | | | $0.5TiB_2$ | 2 |
| | Fe-30Al | 17.2 | | | | | 12 |
| | Fe-28Al | 15.8 | | | | | 4 |
| | Fe-35Al | 20.6 | | | | $0.5TiB_2$ | 98 |
| | Fe-40Al | 24.4 | | | 0.4 | 0.05B | 8 |
| | Fe-38Al | 22.85 | | | 0.4 | 0.05B | 9 |
| | Fe-36.5Al | 21.8 | 24.4 | | 0.4 | 0.05B | 4 |
| | Fe-40Al-2Cr | | 2.0 | | | 0.05B | 6 |
| | Fe-40AlNbC | 24.4 | | | | Nb, C | 2 |
| | 316 SS | | 17.0 | 10.0 | | 2.0Mo-1.0Si-0.08C | 3 |
| | Alloy 800[b] | | 22 | 32 | | | |
| Hafnium | HF-3Al | 3.0 | | | | 0.2Ta-0.005B | 4 |
| Magnesia | MgO | | | | | | 2 |
| Nickel | B-2 | | 0.2 | | | 28.2Mo-1.5Fe-0.2Mn | 4 |
| | HR-160 | | 28.0 | | | 27Co-4Fe-2.8Si-0.5Mo-0.05C | 2 |
| | $Ni_3$ Al | 25.3 | | | | 0.5Hf-0.24B | 11 |
| | NiAl | 50 | | | | | 16 |
| | Ni-45Ti | | | | | 45Ti | 2 |
| Tantalum | T-111 | | | | | 10W-1Hf | 2 |
| Titanium | Ti-Al | 50 | | | | | 1 |
| Zirconia | $ZrO_3$-3MgO | | | | | | 3 |

[a]FG $Al_2O_3$ served as matrix material; SiC in form of whiskers.

[b]Exposed only at APCI; some specimens were analyzed at ORNL.

# RESULTS

## WEIGHT CHANGE MEASUREMENTS

As shown in Table 1, a broad scope of materials was examined during the first phase of these studies. The average weight change in 24 h per unit surface area of a specimen exposed to $(Na,K)NO_3$-1% $Na_2O_2$ at 650°C was used as the initial figure of merit to qualitatively determine a particular material's resistance to corrosion in the molten nitrate salt environment. Such measurements determined whether a particular material should be subjected to more detailed examination. The average 24-h weight changes in this and other nitrate salt environments are shown in Tables 2-4 for pure metals, alloys, and bulk ceramics, respectively. Very large weight losses or gains (>100 g/m$^2$) indicate severe corrosion regardless of the particular type(s) of reaction by which the process proceeded. (Note that, with the exception of one T-111 specimen, no large weight gains were measured in this study.)

**Table 2. Weight changes of pure metals exposed to nitrate salt at 650°C for ~24 h**

| Metal | Salt condition[a] | Weight change[b] (g/m$^2$) |
|---|---|---|
| Cobalt | B1 | -4037 ± 3314 |
| Iron | A1 | +73.5 ± 73.3 |
| | B2 | -40.1 |
| Hafnium | B1 | +1.3 ± 4.5 |
| | C1 | +8.5 ± 4.1 |
| Titanium | B1 | -694 ± 648 |
| Zirconium | B1 | +12.4 ± 1.5 |
| | C1 | +15.2 ± 1.4 |

[a]See experimental procedures section for explanation of salt designations.

[b]Large standard deviations apparently due to formation of extended oxidized regions that often, but not always, spall or detach during exposure or specimen cleaning.

**Table 3. Weight changes of alloys exposed to molten nitrate salt at 650°C for ~24 h**

| Alloy | Salt condition[a] | Weight changes ($g/m^2$) |
|---|---|---|
| Alloy 600 | B1 | -263 |
| | C1 | -149 ± 52.5 |
| NiMo | B1 | -354 ± 74 |
| Ni-45Ti | B1 | -893 ± 160 |
| TiAl | B1 | -236 |
| Hf-3Al | B1 | +4.6 ± 0.5 |
| $Ni_3Al$ | B1 | -54.8 ± 27.7 |
| | C1 | -5.8 ± 10.8 |
| NiAl | B1 | -12.6 ± 5.1 |
| Fe-32Ni-32Al | B1 | -30.0 ± 24.0 |
| Fe-26Al | B1 | -205 ± 37 |
| Fe-28Al | B1 | -87.4 ± 45.9 |
| Fe-30Al | B1 | -25.8 ± 32.1 |
| | B2 | -50.5 ± 9.7 |
| Fe-35Al | A1 | -10.5 ± 4.0 |
| | A2 | -24.8 ± 12.5 |
| | B1 | -19.6 ± 10.8 |
| | B2 | -70.9 ± 28.3 |
| | C2 | -34.2 ± 19.9 |
| Fe-36.5Al | A1 | -1.9 |
| | B2 | -77.3 ± 80.2 |
| Fe-38Al | A1 | +0.1 |
| | B1 | -29.6 ± 41.7 |
| Fe-40Al | A1 | -3.7 ± 0.5 |
| | B1 | -31.3 ± 19.8 |
| Fe-40Al-2Cr | B1 | -19.9 ± 17.6 |
| | B2 | -40.1 |
| Fe-40AlNbC | B1 | -13.3 ± 8.2 |
| 316SS | B1 | -225 |
| HR-160 | B2 | -167 ± 28 |
| T-111 | B1 | -381, +130[b] |

[a]See experimental procedures section for explanation of salt designations.

[b]Specimen covered with thick white product.

**Table 4. Weight changes of bulk ceramics exposed to nitrate salt at 650°C for ~24 h**

| Material | Salt condition[a] | Weight change ($g/m^2$) |
|---|---|---|
| $Al_2O_3$[b] | B2 | -8.2 (± 2.7) |
| | C2 | -1.5 (± 0.1) |
| $Al_2O_3$ - SC[c] | B1 | -2.0 |
| $FGAl_2O_3$[d] | B2 | -11.0 |
| $FGAl_2O_3$ - 10% SiC[e] | B2 | -144 |
| | C2 | -277 |
| $FGAl_2O_3$ - 30% SiC[e] | B2 | -78.5 |
| | C2 | -138 (± 51) |
| $ZrO_3$ (3% MgO) | C2 | +5.1 |
| $ZrO_3$ (3% MgO)[f] | C2 | +3.8 |
| MgO | B1 | -0.9 |
| MgO - SC[c] | B1 | -1.2 |

[a]See experimental procedures section for explanation of salt designations.

[b]Includes data for gel-cast alumina with 0 and 0.05 wt % MgO (Al-08 and Al-35).

[c]SC = single crystal.

[d]Fine-grained (~2 μm) alumina with 0.1 wt % MgO.

[e]SiC in form of whiskers.

[f]50-h exposure.

Based on 24-h weight-change results, the corrosion behavior of the metallic materials could be broadly classified as being in one of four categories: catastrophic degradation by solution and/or rapid oxidation of the solid (e.g., titanium, cobalt); severe attack; moderate to low rates of reaction (as typified by Ni-50Al, iron aluminides, and Zr); and excellent resistance (hafnium). Figure 3 contains representative results for the latter three categories. With respect to the data in

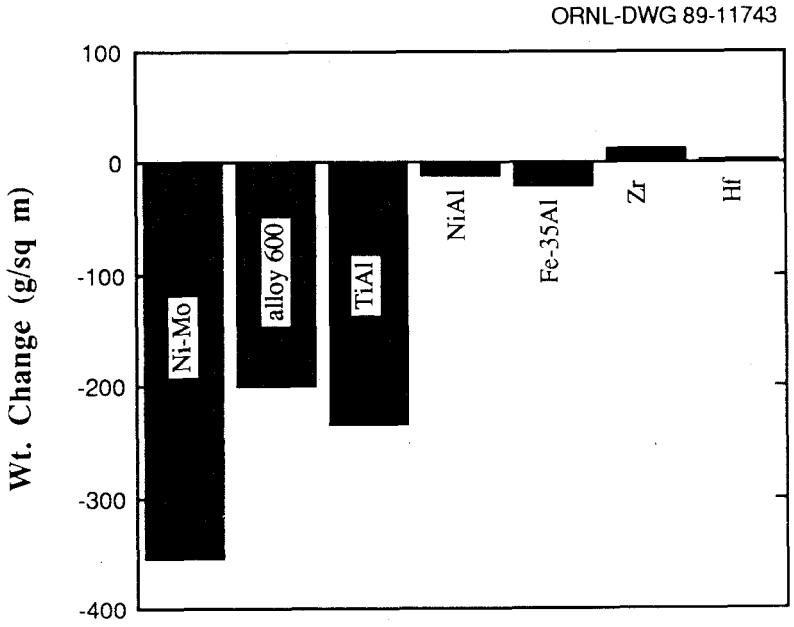


Fig. 3. Average weight change for different materials exposed to $NaNO_3$-$KNO_3$-$Na_2O_2$ at 650°C for ~24 h.

Tables 2 and 3, note that almost all metals and alloys exhibited weight losses, and, with the exception of some of the aluminides, these losses were quite high. Only hafnium and zirconium exhibited weight gains, with the former showing extremely low changes in weight. Most ceramics exhibited relatively small weight changes. However, very high weight losses were observed for several ceramics due to uptake of salt into matrix porosity and subsequent crumbling of the surface region. Such results are not reported in Table 4.

Because iron aluminides appeared to offer an attractive combination of corrosion resistance (based on the above 24-h weight change data), low raw-material cost, and potential fabricability (relative to the attractive ceramics) for applications involving somewhat complex geometries (see "Discussion" section), a relatively large number of iron aluminide specimens have been exposed during the course of these experiments (see Table 1) to determine the compositional and metallurgical conditions necessary for corrosion resistance in this salt

environment. Weight changes of iron aluminides were characterized as a function of aluminum concentration, time, thermomechanical treatment, and salt chemistry.

The influence of salt composition on the corrosion of aluminides (as well as other materials) was quite pronounced. The presence of $Na_2O_2$ in the salt increased the short-term corrosiveness of the nitrate mixture. Figure 4 shows this effect for 24-h weight changes of iron aluminides. However, as shown in Fig. 5, the peroxide effect was short-lived. No increase in weight loss was noted for Fe-35Al specimens exposed for greater than 24 h in a salt with an initial composition of $(Na,K)NO_3$-1% $Na_2O_2$, but high weight losses were measured when the $Na_2O_2$ concentration was refreshed every 24 h (which more closely simulates the MOLTOX condition)[3] during the course of 72-h specimen exposures [Fig. 5(*a*)]. Figure 5(*b*) shows a similar, but less dramatic, difference when the same experiments were performed for Ni-50Al. The weight losses were also a function of the amount of sodium nitrate. Pure $NaNO_3$ was more corrosive than $(Na,K)NO_3$ (see Fig. 6).

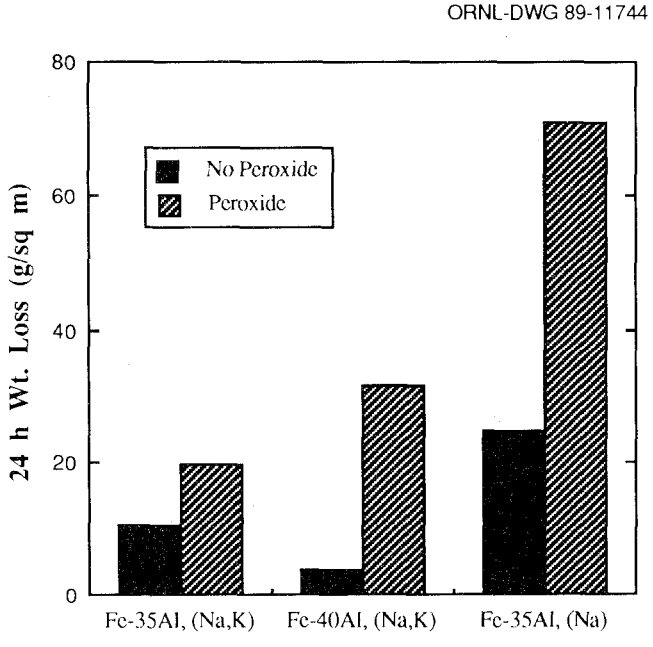


Fig. 4. Average weight change for iron aluminides exposed to $NaNO_3$-$KNO_3$ (Na,K) or $NaNO_3$ (Na) at 650°C for ~24 h (Al concentrations in at. %).

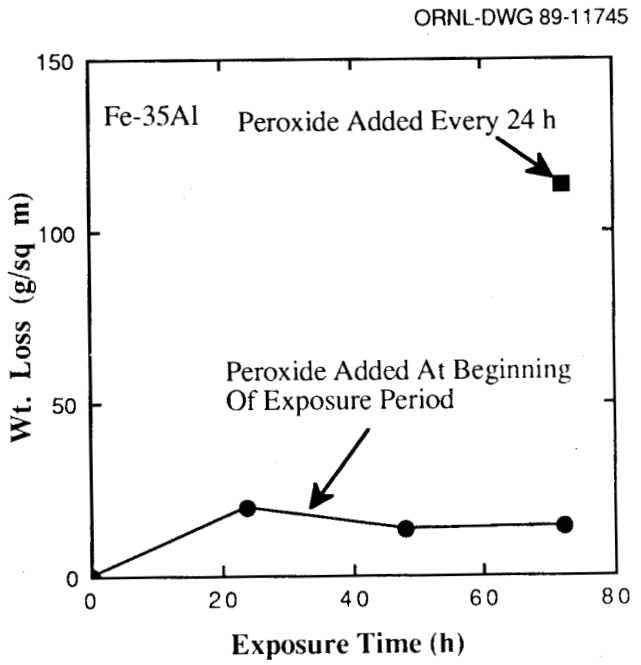


*(a)*

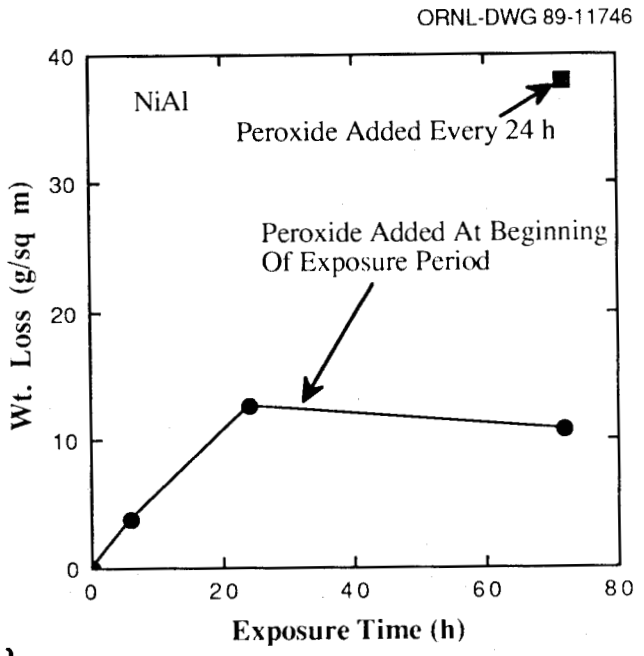


*(b)*

Fig. 5. Weight loss vs exposure time for $NaNO_3$-$KNO_3$(-$Na_2O_2$) at 650°C. (*a*) Fe-35 at. % Al, (*b*) NiAl.

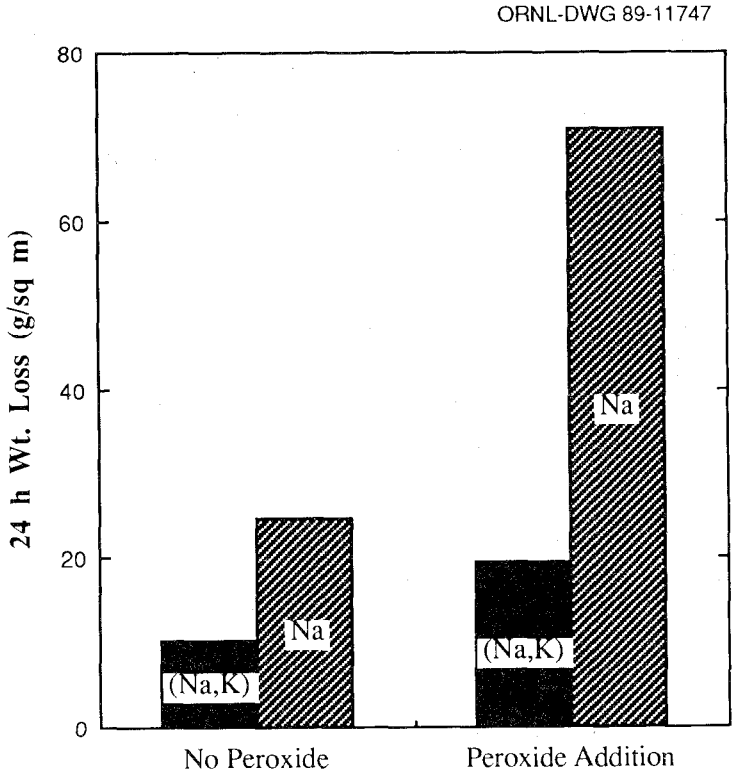


Fig. 6. Average weight change for Fe-35 at. % Al exposed to $NaNO_3$-$KNO_3$-$Na_2O_2$ (Na,K) or $NaNO_3$ (Na) at 650°C for ~24 h.

The weight-loss kinetics for the iron aluminides reflected the diminishing influence of a given peroxide addition with time. As shown in Fig. 5, the rate of weight loss depended strongly on how often peroxide was added to the salt. In different experiments, where the same specimen was cleaned and reexposed to $NaNO_3$-0.4% $Na_2O_2$ several times, a somewhat similar behavior was observed: the rate of weight loss changed only slightly upon reintroduction of a specimen into the salt if no peroxide additions were made but significantly increased when $Na_2O_2$ was added (Fig. 7). When 0.4% $Na_2O_2$ was added at the beginning of each incremental exposure period, approximately linear weight-loss kinetics and an increasing rate with temperature were observed (see Fig. 8). Experiments to determine the effect of temperature in the absence of $Na_2O_2$ additions were not conducted.

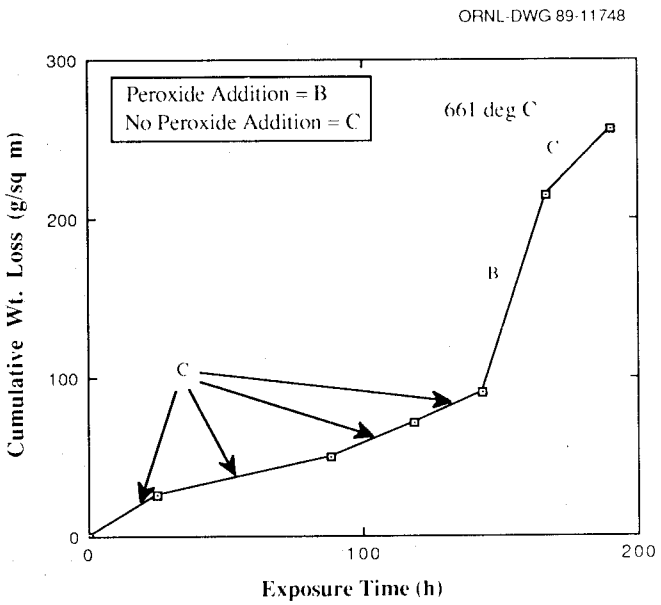


Fig. 7. Cumulative weight losses vs time for Fe-35 at. % Al exposed to $(Na,K)NO_3$(-1 mol % $Na_2O_2$) at 661°C for salt conditions B (peroxide added at start of exposure interval) and C (no new peroxide added).

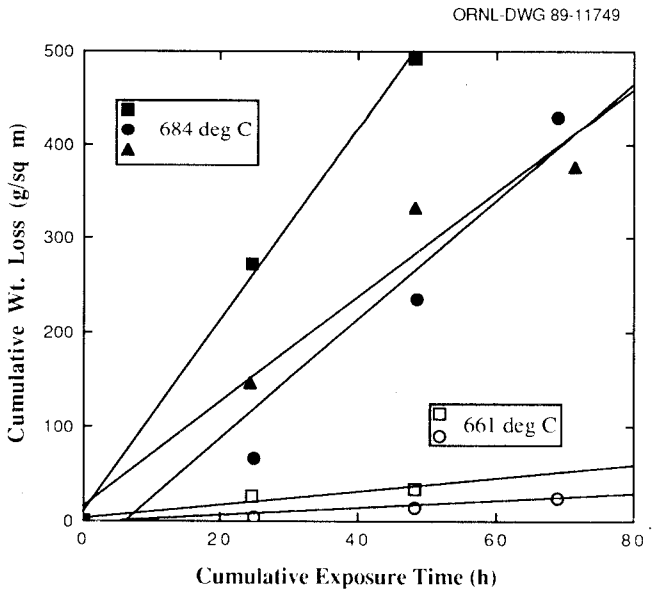


Fig. 8. Cumulative weight losses vs time for Fe-35 at. % Al exposed to $NaNO_3$-$KNO_3$-1% $Na_2O_2$ at 661 and 684°C. Peroxide was refreshed during each exposure segment.

As shown in Table 3, the weight losses of iron aluminide decreased with increasing concentration of aluminum from 26 to about 35 at. % Al (see Fig. 9). As noted above, $NaNO_3$ was more corrosive than $NaNO_3$-$KNO_3$, but in both cases, the weight losses were relatively low above 30 at. % Al. The presence of a preformed $Al_2O_3$ layer (established by exposure at 1050°C in air for 24 h) did not dramatically affect the corrosion of either $Ni_3Al$ or Ni-50Al (Fig. 10), although a slight decrease in weight loss was noted for both of these aluminides. Preliminary data showed no significant effect of preoxidation on Fe-35Al. No important differences in weight changes between annealed and as-rolled specimens of Fe-35Al, $Ni_3Al$, and Ni-50Al were observed.

ORNL-DWG 89-11750

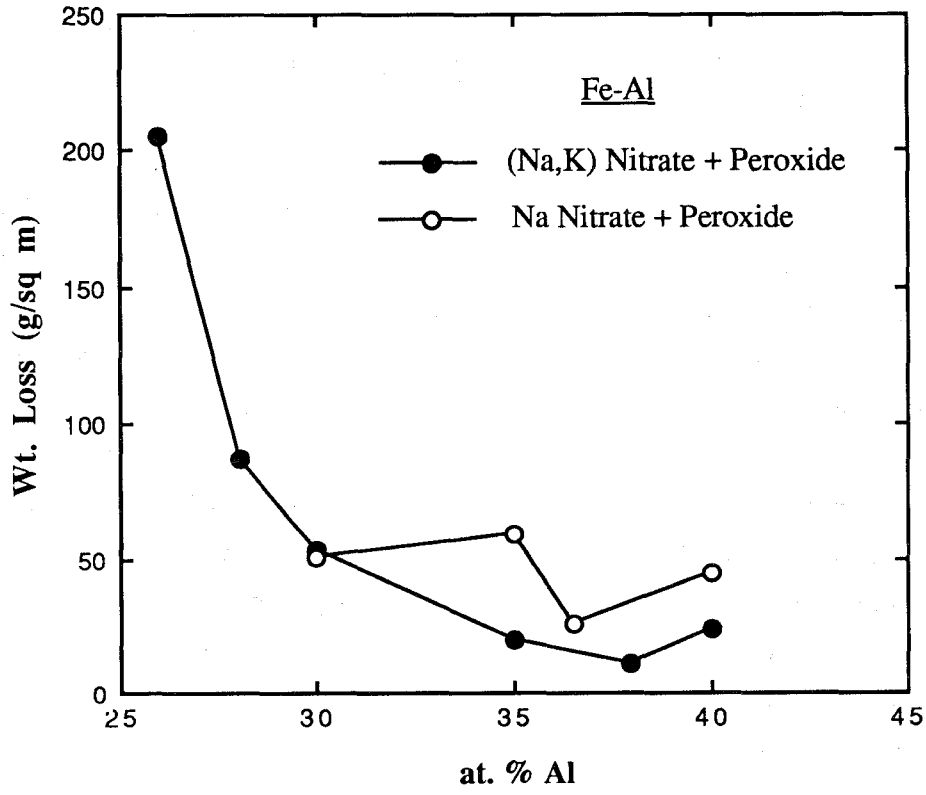


Fig. 9. Average weight change as a function of aluminum concentration for iron aluminides exposed to $NaNO_3$-$KNO_3$-$Na_2O_2$ or $NaNO_3$-$Na_2O_2$ at 650°C for 20 to 30 h.

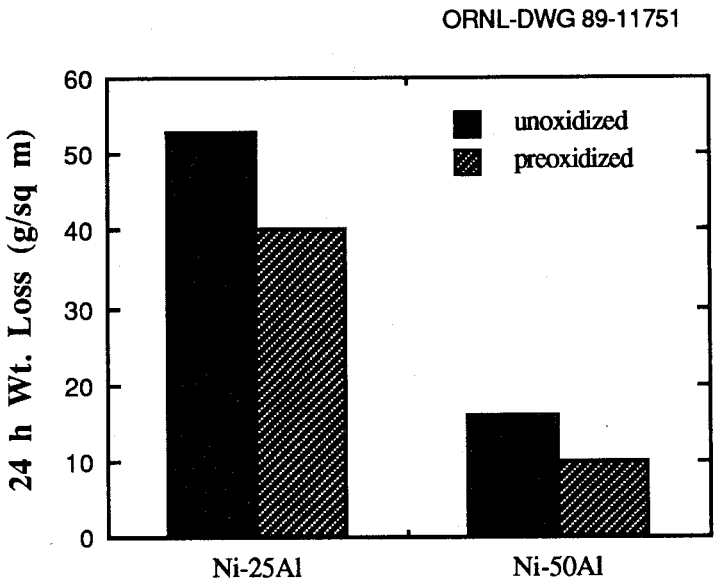


Fig. 10. Average weight losses of $Ni_3Al$ and NiAl exposed to $NaNO_3$-$KNO_3$-$Na_2O_2$ at 650°C for ~24 h.

Because zirconium and zirconia had good corrosion resistance in nitrate salt (see Tables 2 and 4), the viability of using zirconia coatings to improve the resistance of aluminides was investigated. Coatings on both $Ni_3Al$ and NiAl were deposited (courtesy of METCO) by plasma spraying using yttria-stabilized zirconia powder (METCO 204NS) and a NiAl bond coat. The coatings appeared to be adherent, but weight changes after 24-h exposures to the salt were significantly higher than those measured for the uncoated nickel aluminides (Fig. 11). The poor performance appeared to be related to the porosity of the coatings and subsequent lack of integrity due to salt uptake, although the presence of (unknown) impurities in the coatings may have also been a contributing factor.

## MICROSTRUCTURAL ANALYSES

In crucible exposures, APCI had found that the corrosion rate of nickel decreased as the purity of the exposed material increased from

ORNL-DWG 89-11752

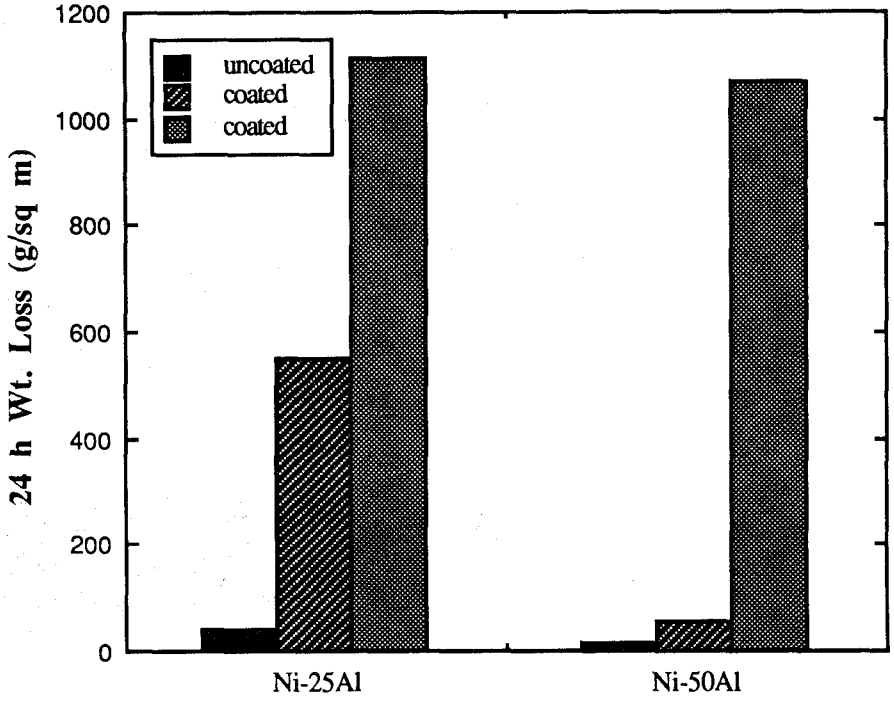


Fig. 11. Weight losses of $Ni_3Al$ and NiAl exposed to $NaNO_3$-$KNO_3$-$Na_2O_2$ at 650°C for ~24 h. Uncoated data represent averages; values for coated specimens are for individual specimens with yttrium-stabilized zirconate coatings deposited by plasma spraying.

99 to 99.9975% (but the rate for the purest form of nickel was still unacceptably high).[17] ORNL analysis of polished cross sections (which were prepared under special dry polishing conditions) showed that extensive intergranular corrosion of Ni-200 and Ni-270 had occurred, but this type of attack was absent when high-purity nickel was exposed in the APCI test (see Fig. 12). Careful microprobe examination of a Ni-200 specimen showed some localization of sulfur and manganese at unopened grain boundaries, but, as shown by APCI weight change data[17] and the microstructural results (Fig. 12), the overall sulfur concentration of the starting material was not directly related to the occurrence of intergranular attack. (The manganese concentrations of the different nickel materials were unknown.)

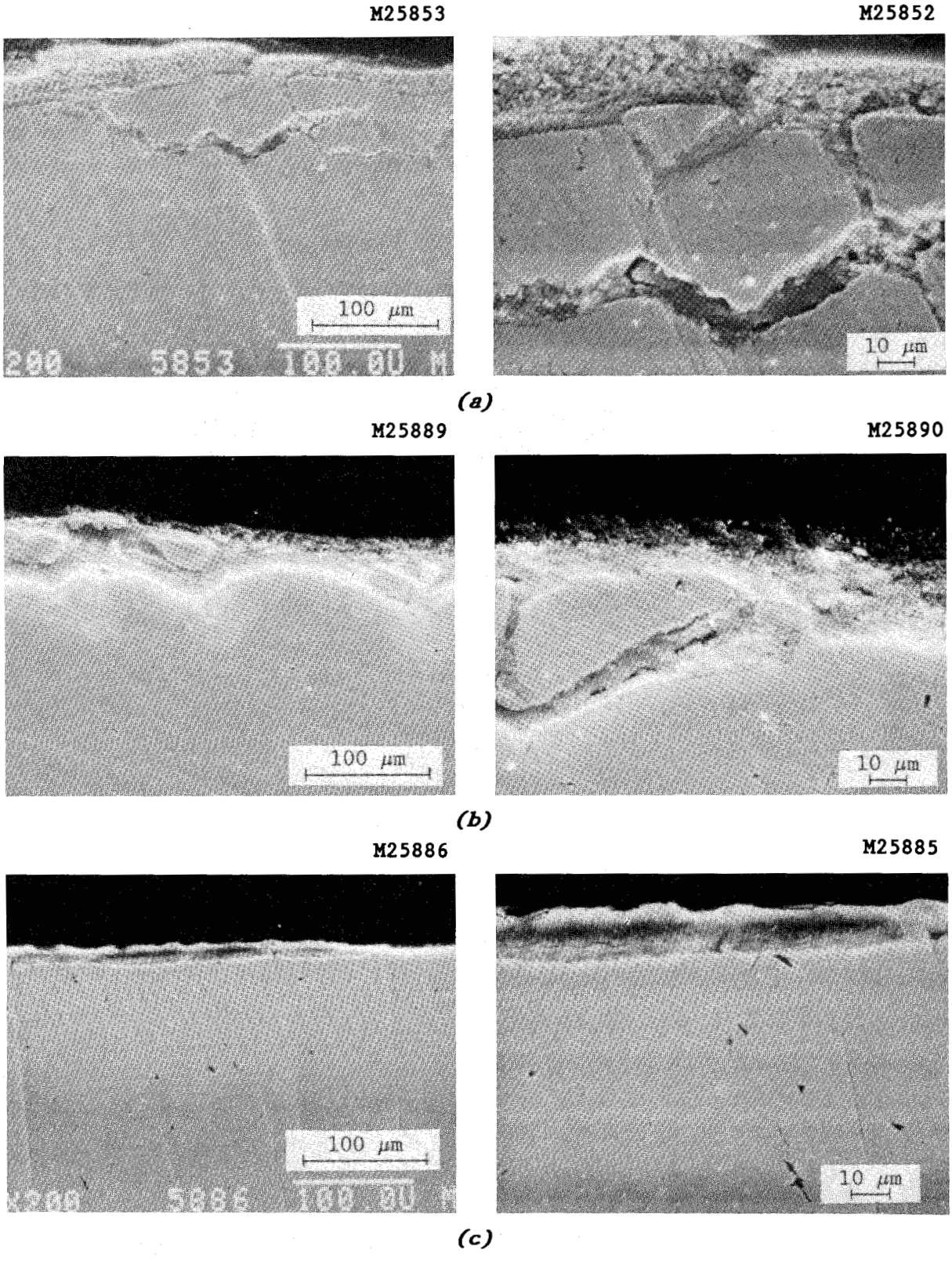


Fig. 12. Polished cross sections of specimens exposed for about 48 h to static $NaNO_3$-$KNO_3$-$Na_2O_2$ at 650°C at APCI; (*a*) Ni-200, 99.0 Ni, 0.075 C, 0.0007 S (wt %); (*b*) Ni-270, 99.97 Ni, 0.02 C, 0.0013 S; (*c*) high purity Ni, 99.9975 Ni, 0.0073 C, 0.0019 S.

$Ni_3Al$ (IC-50) was exposed to nitrate salt at APCI[17] and then analyzed at ORNL. Scanning electron micrographs of specially (dry) polished cross sections of both as-wrought and preoxidized $Ni_3Al$ exposed to Salt 1 at 650°C for about 48 h are shown in Fig. 13. Associated EDX showed that a thin surface layer on both specimens was enriched in aluminum relative to the unaffected underlying matrix and also contained some sodium. The intergranular oxidation seen in Fig. 13(*b*) was not due to the salt exposure but rather to the high-temperature preoxidation treatment (1050°C in air, 24 h), as described by others.[18-19] Subsequent analyses of nickel aluminide exposed in the ORNL molten salt facility also revealed the presence of an aluminum-enriched surface layer.

Specimens of the nickel-based alloy 600 exposed to the molten nitrate salt under sparged crucible conditions at ORNL and in the APCI MOLTOX pilot plant were examined. The alloy 600 exposed at ORNL [which suffered a weight loss of 263 $g/m^2$ in 24 h with salt condition B1 (see Table 3)] had a thin surface layer (see Fig. 14) that was depleted in chromium relative to the starting composition (as determined by EDX). Chromium depletion was also detected for an alloy 600 specimen from the more aggressive environment of the pilot plant's desorber (Fig. 15) as well as for a similarly exposed alloy 800 (Fig. 16). Table 5 lists the ratio of chromium concentration in the surface layer to that in the bulk for the specimens shown in Figs. 14–16. Note that, for the cross sections shown in Figs. 15 and 16 as well as in many others, the observed region next to the clearly defined edge is not wholly a corrosion product layer; in many cases it is mainly composed of the residual salt when a specimen was polished dry without cleaning its surface. Sometimes, the specimen mounting material would "pull" away from the specimen creating a gap that became filled with polishing compound during metallographic preparation. In other cases, the polishing process led to localized melting of the salt layer. Such preparation problems often led to unusual structures and difficulties in analyses.

M25851

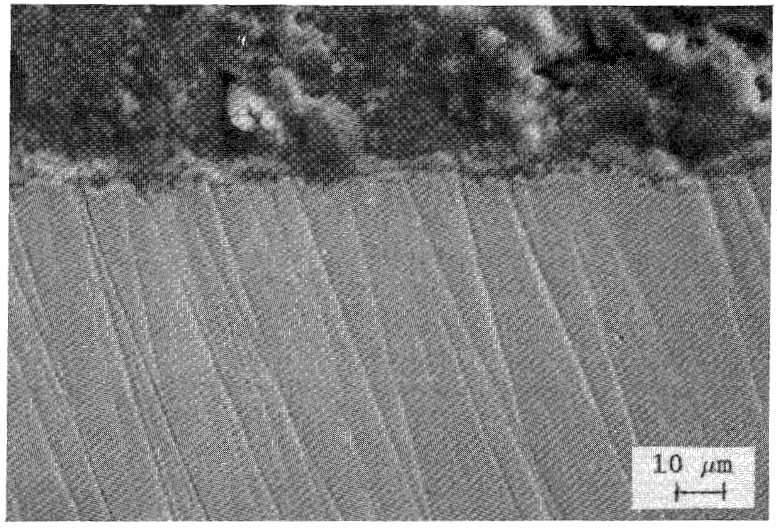


*(a)*

M25878

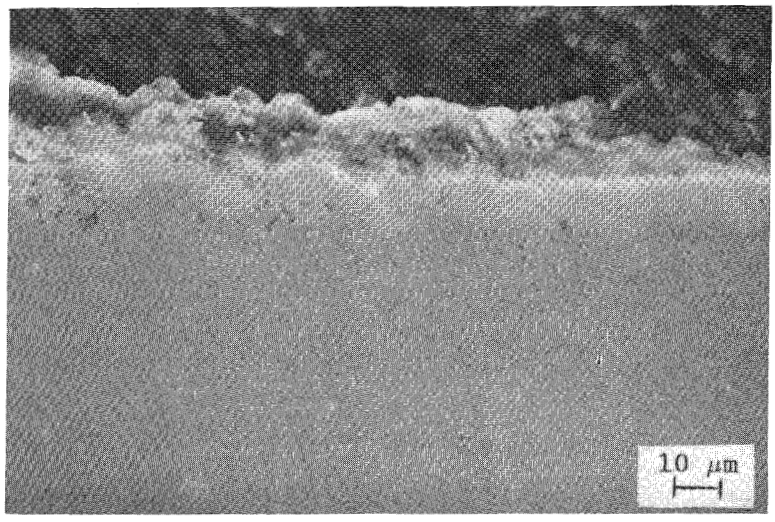


*(b)*

Fig. 13. Polished cross sections of $Ni_3Al$ exposed for about 48 h to static $NaNO_3$-$KNO_3$-$Na_2O_2$ at 650°C at APCI; (*a*) as-wrought; (*b*) preoxidized.

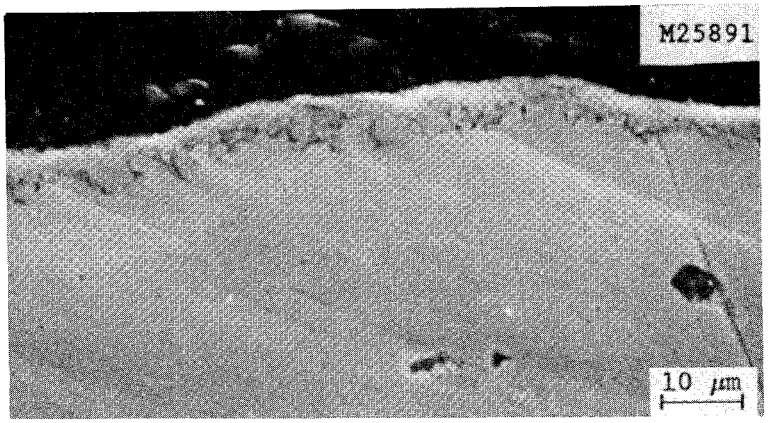


Fig. 14. Polished cross section of alloy 600 exposed to $NaNO_3$-$KNO_3$-$Na_2O_2$ for 24 h at 650°C.

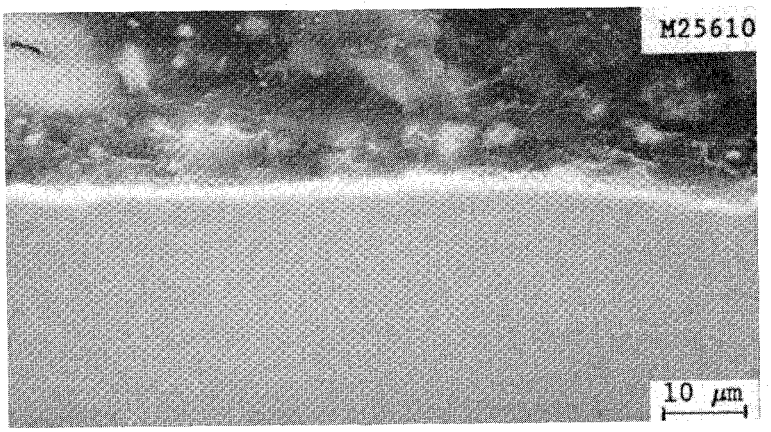


Fig. 15. Polished cross section of alloy 600 exposed in MOLTOX pilot plant at 650°C.

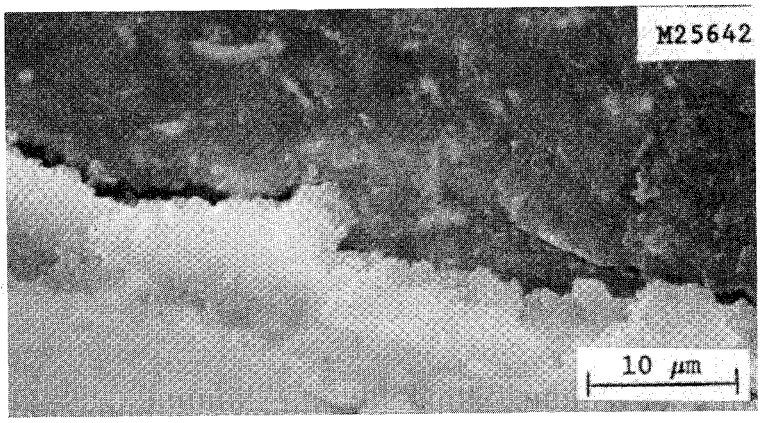


Fig. 16. Polished cross section of alloy 800 exposed in MOLTOX pilot plant at 650°C.

**Table 5. Ratio of chromium concentration in thin surface layer to bulk chromium concentration for alloys exposed to $(Na,K)NO_3$-$Na_2O_2$ at 650°C**

| Alloy | Salt condition | Cr(surface):Cr(bulk)[a] |
|---|---|---|
| 600 | B1 | 0.4 |
| 600 | PP[b] | 0.5 |
| 800 | PP[b] | 0.3 |

[a]As determined by semiquantitative analysis of energy-dispersive X-ray spectroscopy data.

[b]Exposed in MOLTOX pilot plant.

An aluminized alloy 800 specimen that was exposed in the APCI pilot plant was also analyzed at ORNL. Examination of as-aluminized materials (but unexposed to salt) revealed a two-layer structure schematically depicted in Fig. 17. The outer zone was highly enriched in aluminum and, as a consequence, frequently cracked. The inner layer consisted of two phases: an aluminide and a matrix with a much lower aluminum concentration. When the aluminized alloy 800 was exposed to the nitrate salt in the pilot plant, the cracked outer layer permitted the salt to reach the interface between the two zones and resulted in corrosion at more than one surface (see Fig. 18). An elemental electron microprobe image map of this region (Fig. 19) clearly revealed the two-phase nature of the inner layer, the high aluminum content of the outer zone, the ingress of salt to the interface between the aluminized layers (note the presence of sodium and concentrated oxygen), and the existence of products involving aluminum and iron in the trapped salt. There also was some evidence of a Na-Cr-O reaction product in the underside of the outer layer.

ORNL-DWG 89-11753

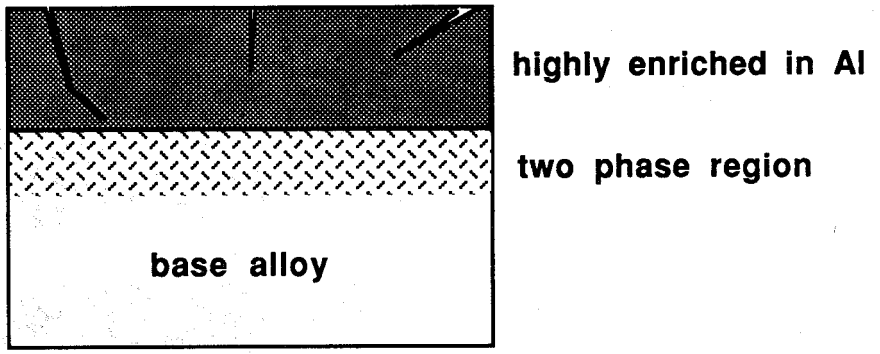


Fig. 17. Schematic drawing of heavily aluminized Fe-Ni-Cr or Ni-Cr-Fe alloy based on microstructural analysis of unexposed aluminized alloy 800 and type 316 stainless steel.

M25074

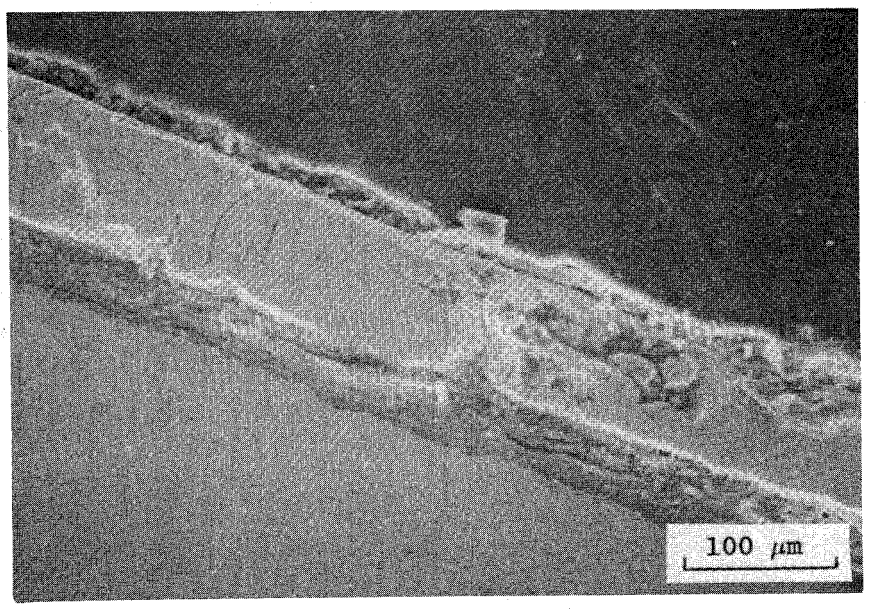


Fig. 18. Polished cross section of aluminized alloy 800 exposed in MOLTOX pilot plant at 650°C.

YP8657

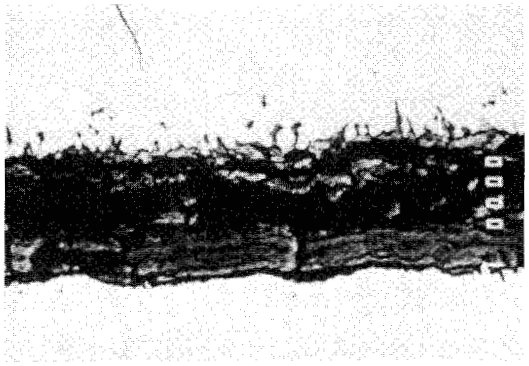

Backscattered Electron Image

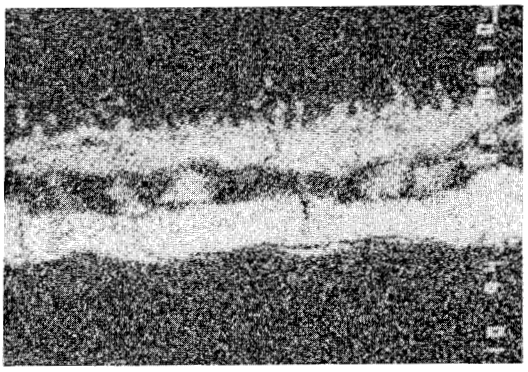

Oxygen

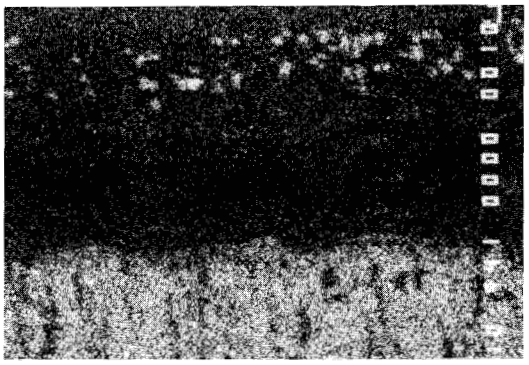

Chromium

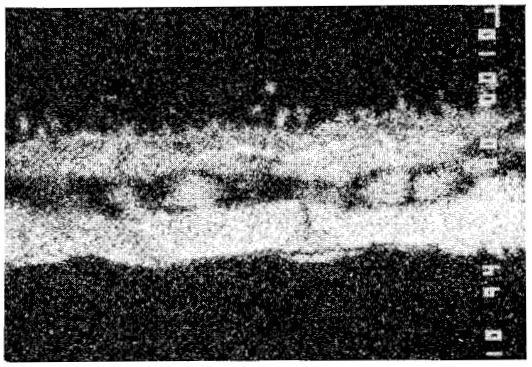

Sodium

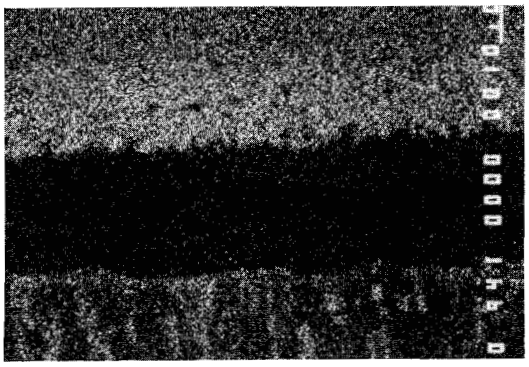

Nickel

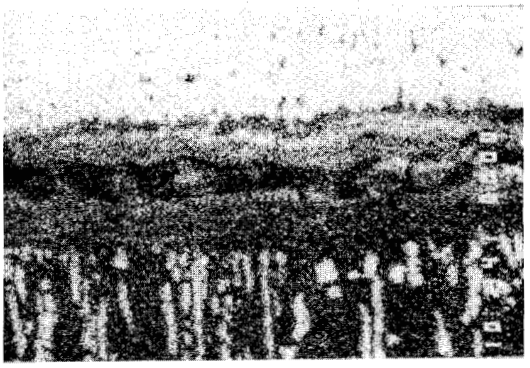

Aluminum

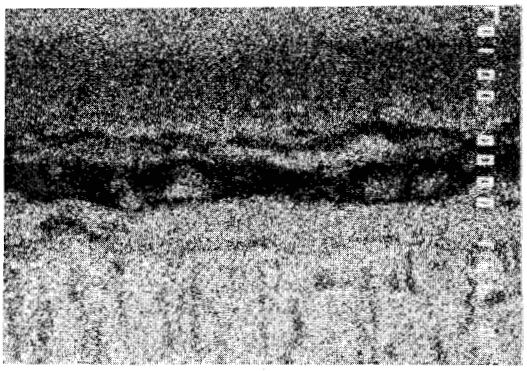

Iron

Fig. 19. Elemental X-ray maps from polished cross section of aluminized alloy 800 exposed in MOLTOX pilot plant at 650°C.

Examination of an aluminized type 316 stainless steel exposed at 510°C in the pilot plant absorber region revealed little evidence for the presence of an aluminum-rich layer from the aluminization process (see Fig. 20). Aside from residual salt still on the surface, some apparent corrosion products consisting of iron, aluminum, and possibly sodium were found in a surface layer. A similarly exposed specimen of type 316 stainless steel that was not aluminized exhibited the same type of microstructure.

M25137

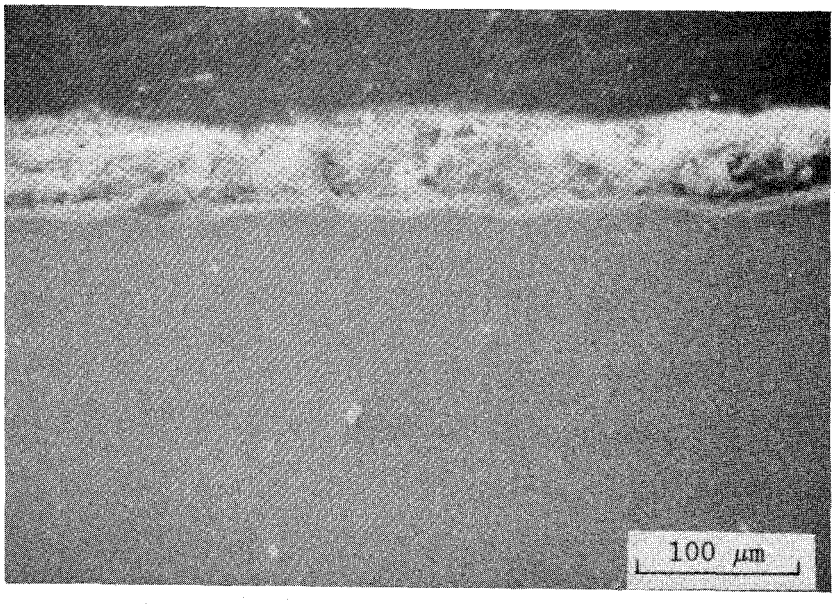


Fig. 20. Polished cross section of aluminized type 316 stainless steel exposed in MOLTOX pilot plant at 510°C.

Examination of polished cross sections of a selected number of Fe-35Al specimens exposed at ORNL did not reveal the presence of a contiguous corrosion product (see, for example, Fig. 21) even when care was taken not to remove residual salt from a particular specimen and special polishing procedures were used. However, EDX showed aluminum enrichment along much of the surface that could be associated with the formation of a reaction product (see "Discussion"). Isolated areas of aluminum-enriched material (such as that denoted "A" in Fig. 21) could be found in the salt layer. Aluminum enrichment was also detected by EDX when a cleaned Fe-35Al specimen surface was examined in normal view (rather than as a cross section).

M28359

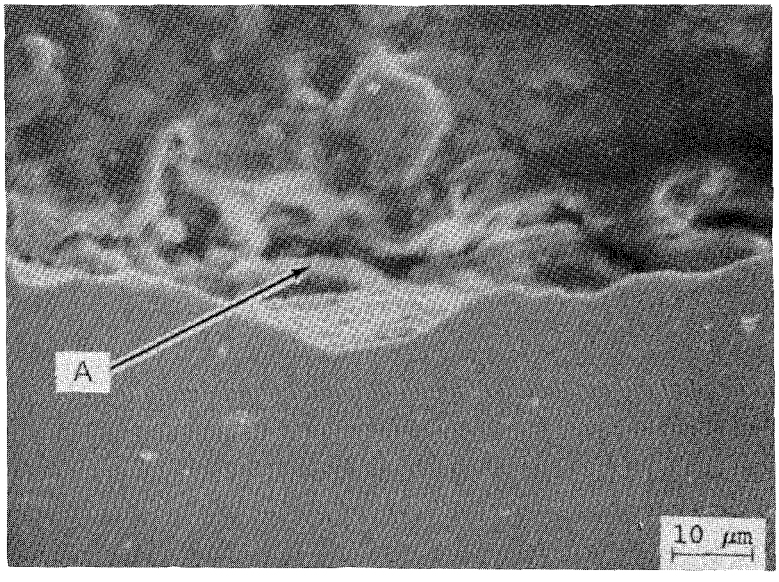


Fig. 21. Polished cross section of Fe-35 at. % Al exposed to $NaNO_3$-$KNO_3$-$Na_2O_2$ for 24 h at 650°C.

Unlike the aluminum- or chromium-containing materials, zirconium formed a well-defined corrosion product morphology upon exposure to the molten nitrate salt. As shown in Fig. 22, multiple surface layers formed under the typical salt condition ($NaNO_3$-$KNO_3$-$Na_2O_2$, B1) and also when the zirconium was exposed to $NaNO_3$-$KNO_3$ in an open crucible (Fig. 23). The B1 condition led to a slightly greater depth of reaction as well as a correspondingly higher weight gain (11.1 vs 9.9 g/m$^2$). Indeed, although reaction depths could not be measured accurately because of the cracking of the product layer (see Figs. 22 and 23), the measured weight gains tracked with thickness of the product layer for exposures (crucible open to air) up to 760 h (Fig. 24). The reaction layers on zirconium exposed under these open-crucible conditions for more extended time periods are shown in Fig. 25, while Fig. 26 contains the thickness data versus exposure time gotten from all the metallographic observations. Hafnium appeared to form a somewhat thinner product layer than zirconium (Fig. 27), consistent with its smaller weight gain (see Fig. 3).

## DISCUSSION

As demonstrated previously,[6-9] corrosion in molten nitrate salts can result both from solid-state oxidation of the base metal and from solubility-driven dissolution reactions. With competing reactions of dissolution and corrosion product formation, the significance of net weight-change measurements must be carefully considered in the analysis of results. The measured weight change $w$ can be expressed as

$$w = w_o - w_s - w_d \quad , \tag{1}$$

where $w_s$ is the absolute value of the weight loss due to dissolution of metal ions into the salt, $w_o$ is the gain due to uptake of oxygen by the specimen, and $w_d$ is the weight change caused by removal of any (or all) of the surface reaction product when rinsing the salt from the specimen after exposure (descaling) and/or by mechanical scale detachment during cooling from the exposure temperature (spallation). Large weight losses

Y210143

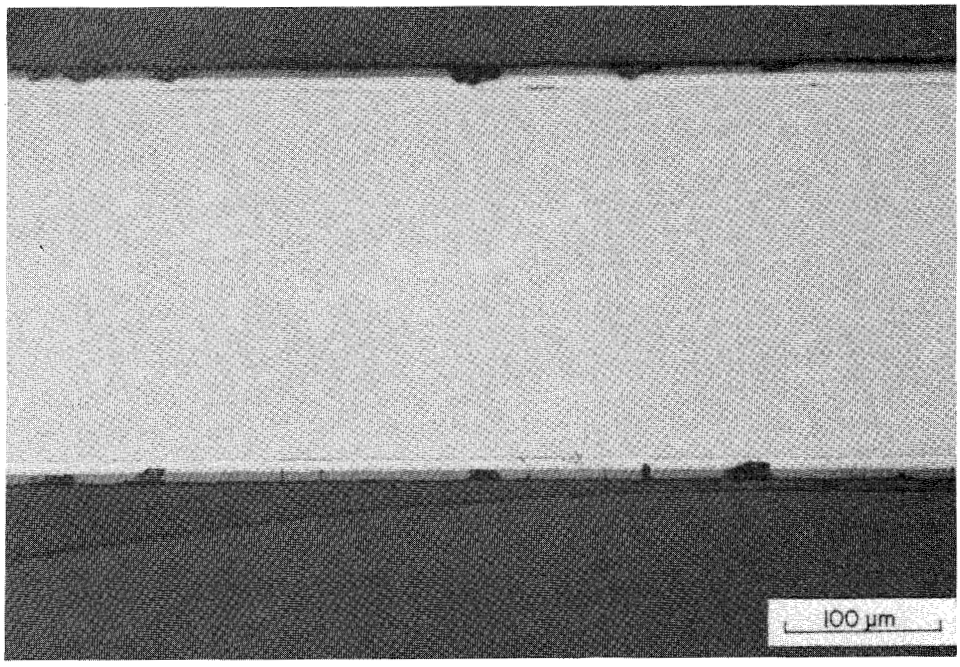


Y210144

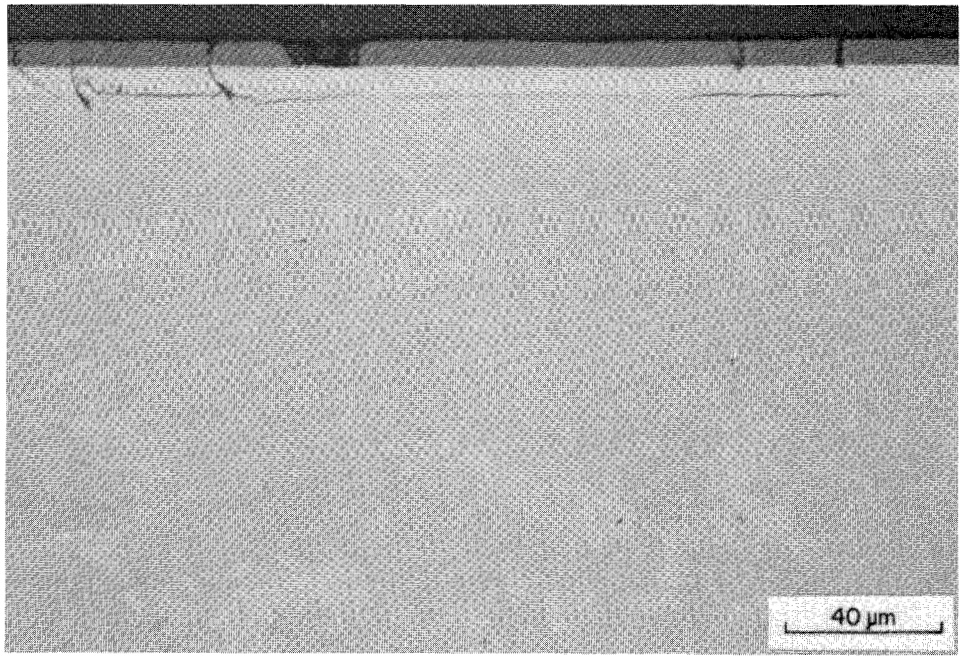


Fig. 22. Polished cross section of zirconium exposed to $NaNO_3$-$KNO_3$-$Na_2O_2$ for 23.5 h at 650°C.

Y210131

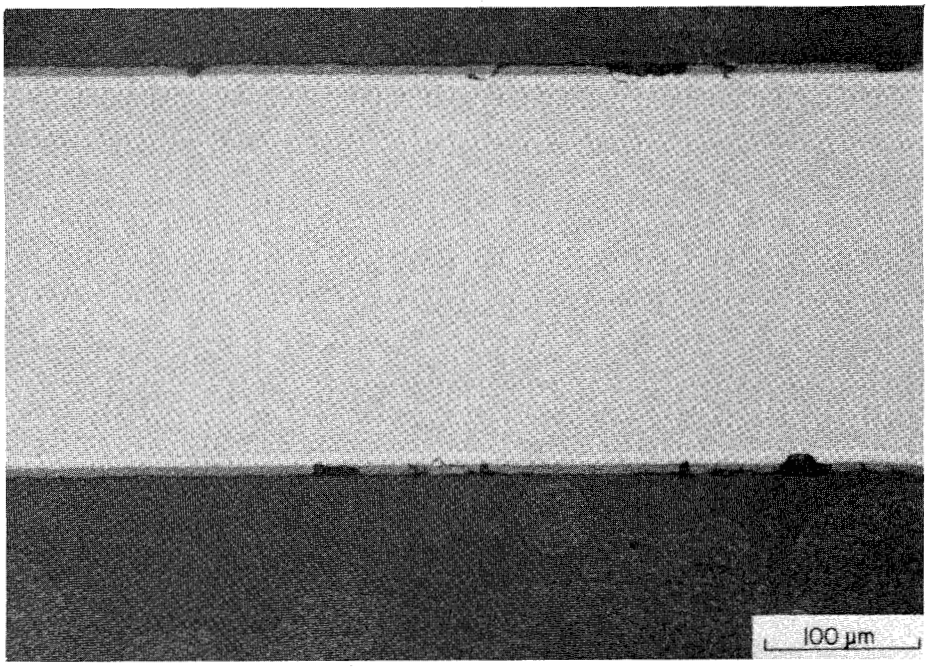


Y210132

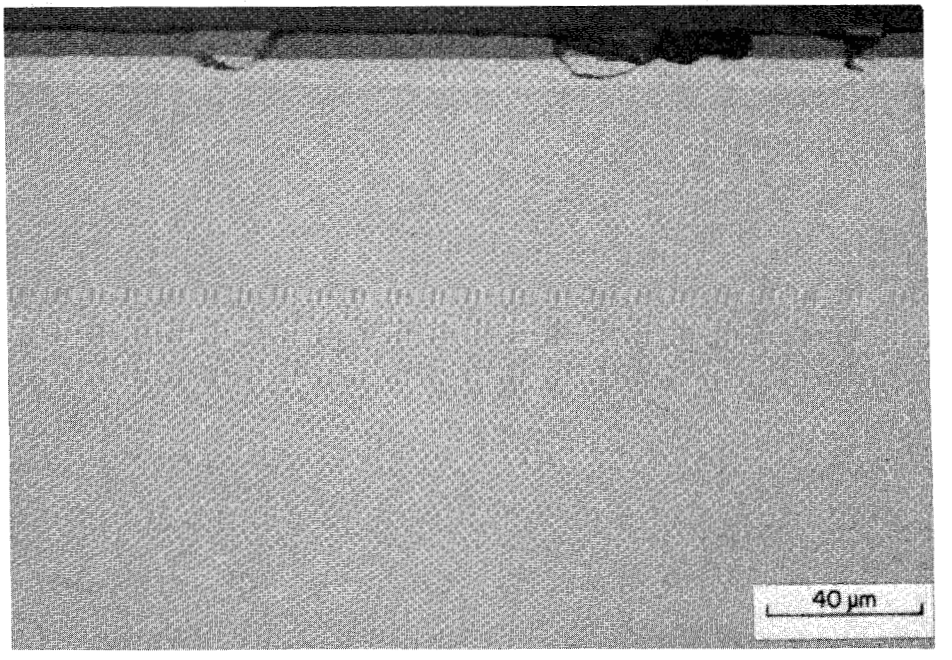


Fig. 23. Polished cross section of zirconium exposed to $NaNO_3$-$KNO_3$-$Na_2O_2$ in air for 24 h at 650°C.

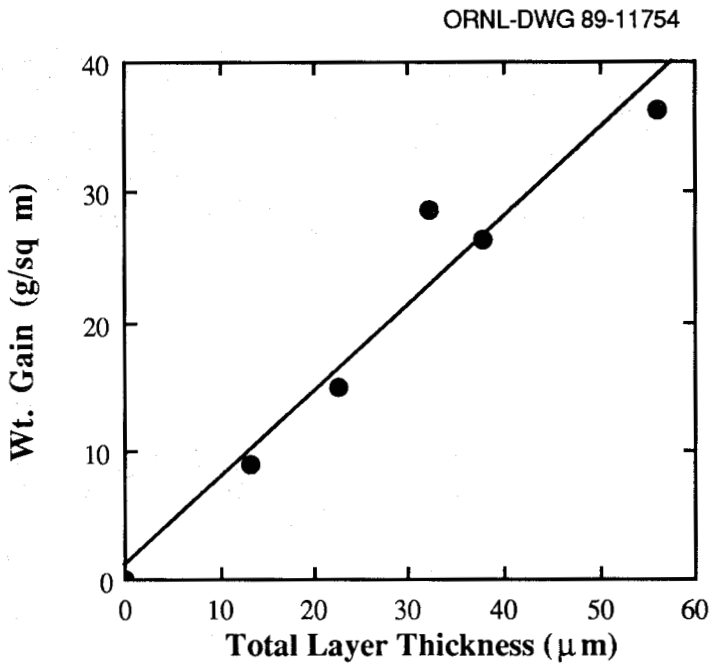


Fig. 24. Measured weight gains vs total layer thickness for zirconium exposed to nitrate salt in air at 650°C.

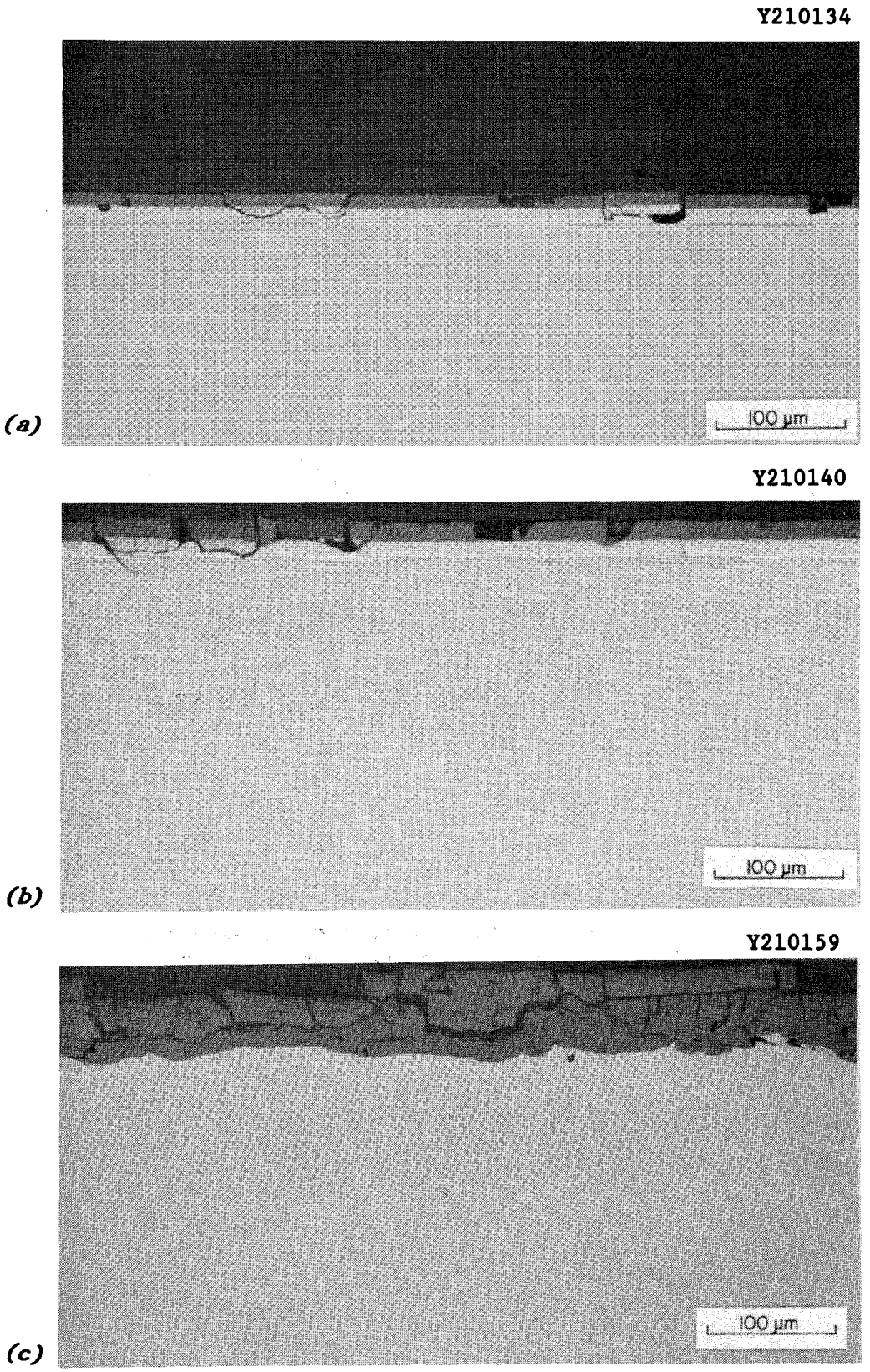


Fig. 25. Polished cross section of zirconium exposed to $NaNO_3$-$KNO_3$-$Na_2O_2$ in air at 650°C; (*a*) 96 h, (*b*) 305 h, (*c*) 760 h.

ORNL-DWG 89-11757

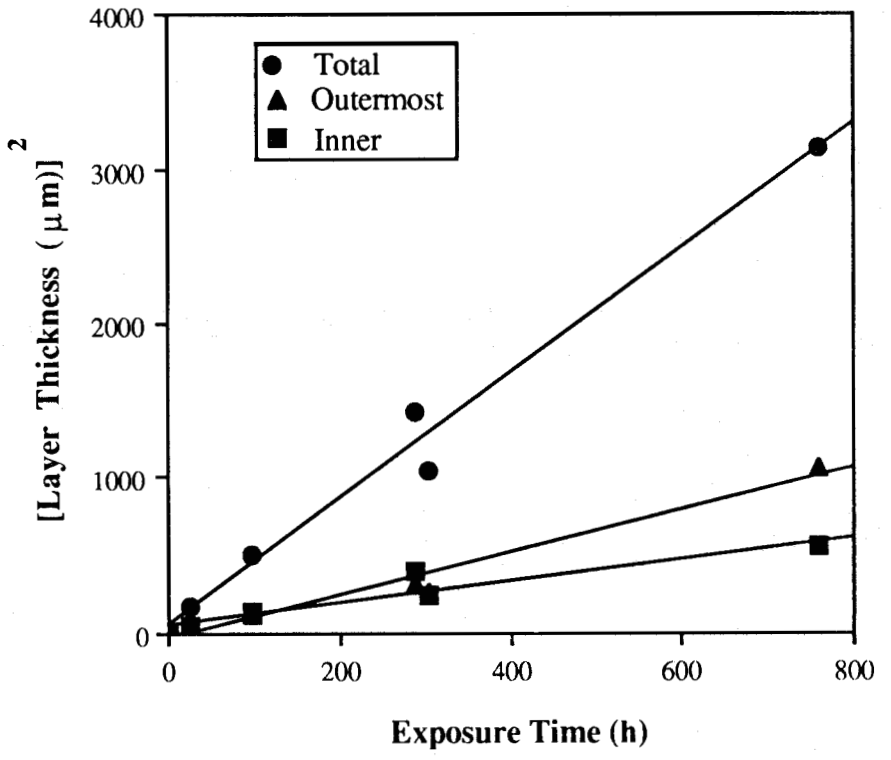


Fig. 26. Square of layer thickness vs exposure time for zirconium exposed to nitrate salt in air at 650°C.

Y210150

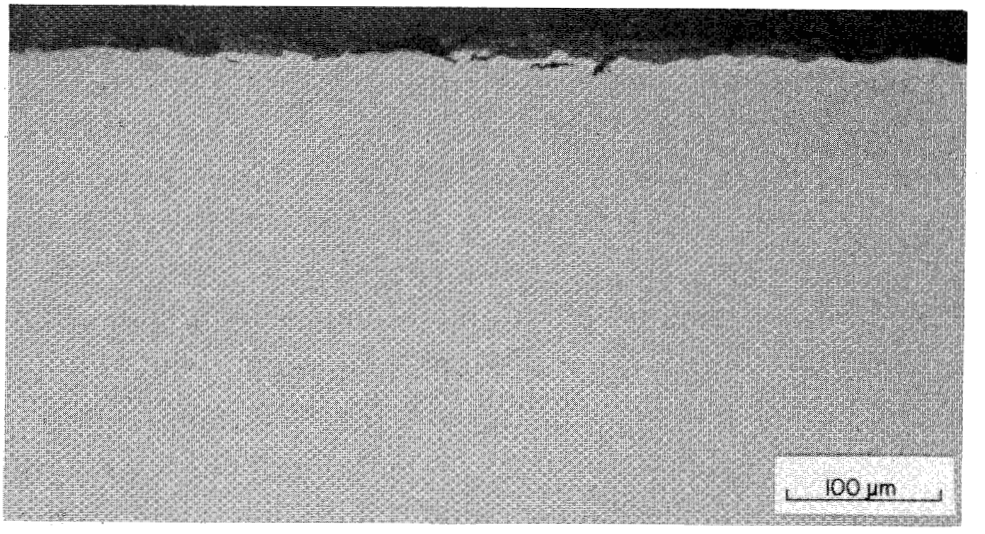


*(a)*

Y210156

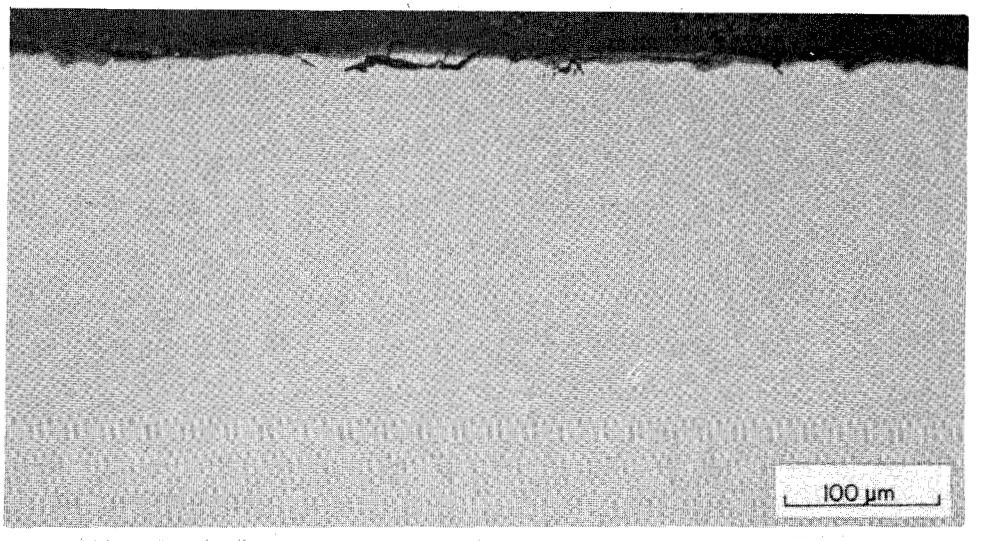


*(b)*

Fig. 27. Polished cross sections of hafnium exposed to $NaNO_3$-$KNO_3$-$Na_2O_2$ at 650°C; (*a*) 24 h, (*b*) 39.6 h.

(negative $w$) thus indicate significant corrosive attack, but, by themselves, do not distinguish between that caused by dissolution (weight loss during exposure) and scaling (weight gain followed by loss due to descaling/spallation). Excessive weight gains would also be indicative of corrosion susceptibility that can be associated with oxidation and scale formation. Relatively small weight changes, however, do not necessarily mean a particular material is resistant to corrosion. If both dissolution and oxidation are occurring at rates such that oxygen uptake is approximately offset by metal ion dissolution, the net weight change would be small, while the actual overall corrosion rate is substantial. Thus, considered alone, relatively large weight changes may be able to indicate relative corrosion rankings, but they cannot elucidate the corrosion mechanism. Small weight changes may or may not be significant in ranking materials. In either case, such measurements must be supplemented by thermodynamic and microstructural observations to better understand the corrosion processes and to strictly compare the corrosion resistance of different materials.

The equilibrium phases for Fe-Na-K-N-O and Al-Na-K-N-O as a function of $P_{O_2}$ and $P_{N_2}$ were calculated using the SOLGASMIX program (Figs. 28 and 29) and were combined with thermodynamic and kinetic data in the literature to better interpret the present experimental observations. The calculations underlying the constructions of Figs. 28 and 29 used the best available free energy data for all possible products from these elements, prescribed activities, and assumed ratios of Na:$M$ and K:$M$ ($M$ = Fe or Al) based on recent experience with molten carbonate systems.[20] As shown in Fig. 28 and elsewhere,[11,16] $Fe_2O_3$ should be stable in this salt. Thus, as reported in the present case for nitrate salt without a peroxide addition (Table 2) and by others,[11-14] the exposure of iron should lead to weight gains. Depending on the basicity of the salt, $NaFeO_2$ can form and then be dissolved in the salt.[16] Indeed, this would explain the observation of a weight loss when iron is exposed to nitrate with peroxide (see Table 2 and below) because the presence of $Na_2O_2$ increases the basicity of the nitrate mixture. However, there is only some indirect evidence from the

ORNL-DWG 89-11755

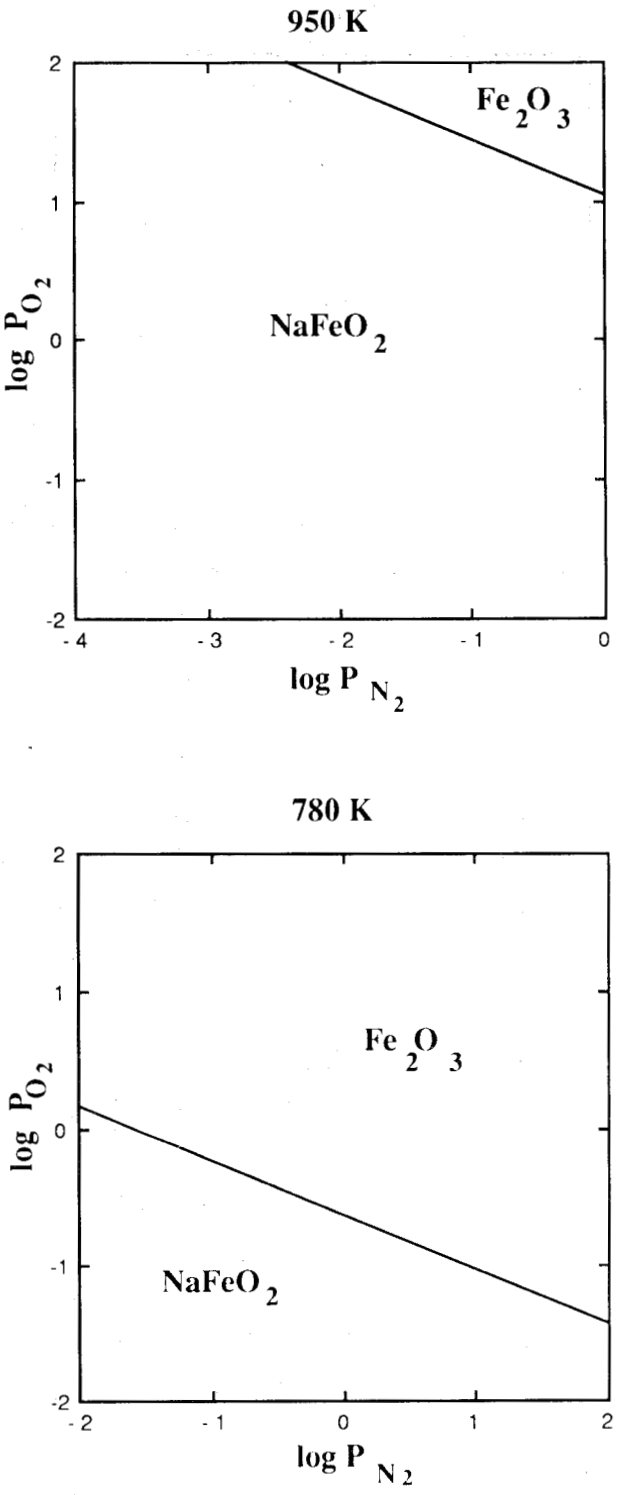


Fig. 28. Phase stability diagram of the Fe-Na-K-N-O-Ar system at 677 and 507°C. The ratio of Na:K:Fe is 50:50:0.01.

ORNL-DWG 89-11756

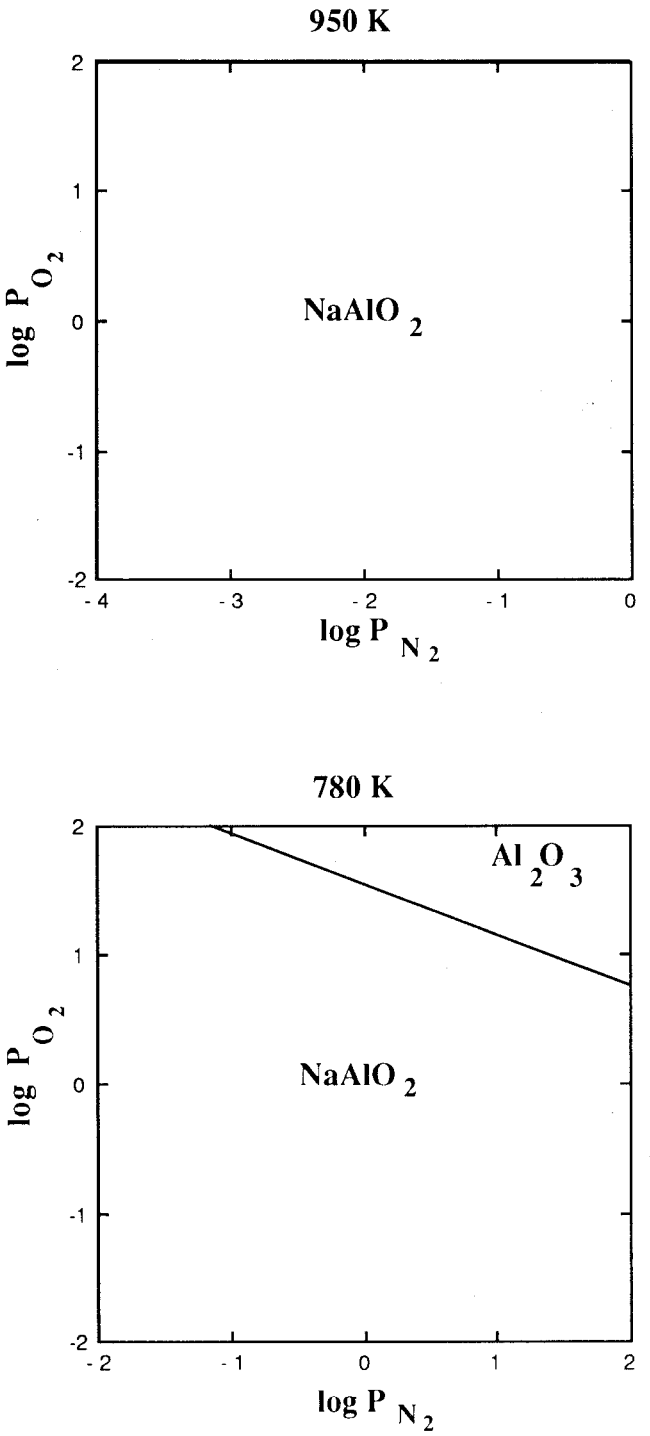


Fig. 29. Phase stability diagram of the Al-Na-K-N-O-Ar system at 677 and 507°C. The ratio of Na:K:Al is 50:50:0.01.

microstructural results that an iron-containing product formed; the elemental X-ray map in Fig. 19 shows some coincidence of iron, oxygen, and sodium concentrations. Previous work on Fe-Ni-Cr alloys in nitrate salt showed that mixed oxides rich in iron formed on exposed surfaces,[6-9] but such layers were not evident in this study (which was conducted at higher temperatures and oftentimes used a different salt chemistry because of the presence of $Na_2O_2$). However, as found in these previous investigations, a depletion in chromium was observed in the surface layers on exposed alloy 800 and alloy 600 (Ni-Cr-Fe) (see Table 5).

The preferential dissolution of chromium ions from Fe-Ni-Cr and Ni-Cr-Fe alloys arises from a high solubility of the chromate and dichromate in the nitrate salt.[6] In addition to the analysis of exposed surfaces, the transfer of chromium out of the solid was evident from measurements of chromium in the salt.[6,9] Such analyses showed that this reaction was greatly accelerated when the temperature of the melt was greater than 625°C. It is therefore not unexpected that materials with significant amounts of chromium will perform poorly in this salt, and the present results reflect this: alloy 600, HR160, and austenitic stainless steel had poor corrosion resistance (Table 3). It is interesting to note that, as the chromate species accumulates in the salt and the acidity of the salt increases, the corrosivity of the melt toward the iron should also increase.[14] This may explain the accelerated corrosion of Fe-Ni-Cr alloys above 625°C and, if so, suggests that the corrosion rate would not decrease with time despite the depletion of the reactive species from the surface.

The lack of corrosion resistance of nickel to the nitrate salt cannot be adequately explained. Nickel is less reactive than iron (mild steel) in $(Na,K)NO_3$ between 250 and 450°C (refs. 13 and 15); and, furthermore, based on analogy with what is known for molten sulfates,[21] NiO should become less soluble as the nitrate salt becomes more basic. While the corrosion of nickel was exacerbated by intergranular attack (Fig. 12), this alone cannot explain the deviation from expected behavior: the specimen that did not show evidence of grain boundary reaction [Fig. 12(*c*)] still suffered a relatively high weight loss in

the APCI experiment.[17] This behavior could be related to impurities in the nickel (possibly carbon[17]) and/or an unidentified oxidation reaction, but the current data are inadequate to address this issue in any detail.

The behavior of aluminum (alumina) in nitrate salt systems is important given the relatively good corrosion resistance of iron aluminides shown in the present study. $NaAlO_2$ should form on exposure of aluminum-containing alloys to the nitrate salt (see Fig. 29) and be less soluble than $Al_2O_3$ in the more basic salt used in the current experiments. Some evidence that $NaAlO_2$ had indeed formed can be seen from the analysis of the aluminized alloy 800 exposed in the APCI pilot plant, where, as shown in Fig. 19, there was a strong correlation between the presence of Na, Al, and O in the region between the outer and inner aluminized layers. The aluminum-rich surface layer on exposed nickel aluminide contained some sodium (and relatively little potassium). On iron aluminide (Fig. 21), some isolated regions concentrated in Na and Al were observed. Also, as described in the "Results" section, aluminized stainless steel and nickel and iron aluminides were found to have thin surface layers characterized by higher relative aluminum concentrations than the underlying metal (but sodium was not detected). Such data may be evidence of an adherent thin $Al_2O_3$ layer such as that found on aluminides exposed to $NaNO_3$-$Na_2O_2$.[22]

The absence of microstructural evidence for an adherent, protective $NaAlO_2$ layer may result from the removal of aluminate during the specimen-cleaning procedure after exposure. This would then lead to a descaling contribution ($w_d$) to the net weight change [see Eq. (1)]. However, when the residual salt is left on a specimen and careful dry polishing techniques are employed, there is still no compelling evidence for a contiguous $NaAlO_2$ scale (see, for example, Fig. 21). The localized areas of sodium and aluminum concentrations may just reflect the presence of aluminate in the frozen salt. Indeed, the "best" evidence for $NaAlO_2$ (Fig. 19) was the case where salt was trapped between the outer and inner surface layers and somewhat isolated from the bulk melt during the experiment. While $NaAlO_2$ can become physically detached during growth or when the specimen is rapidly cooled upon being

pulled from the melt, the observation that weight gains are negative (but relatively small) for bulk alumina (Table 4) may indicate that the corrosion product layer is dissolving (albeit rather slowly) into the salt.

Weight-loss kinetics for aluminides exposed to salt melts periodically refreshed with $Na_2O_2$ were not indicative of the formation of a protective reaction product layer (see Fig. 5). However, as also shown in Fig. 5, when $Na_2O_2$ was added to the salt at the beginning of an extended exposure period and not replenished, weight losses did not increase after about 48 h. Such observations illustrate the importance of the peroxide in reactions associated with the formation and, presumably, the loss of $NaAlO_2$ and $NaFeO_2/Fe_2O_3$ (for iron aluminide). This is not unexpected; solubilities of oxides in the nitrate salt should be highly dependent on salt basicity,[16,21] and it is reasonable that the addition of $Na_2O_2$ should significantly increase the solubility of these oxides in the basic dissolution regime.[21] As noted above, the presence of $Na_2O_2$ in the melt caused the weight change of pure iron to switch from a gain to a loss. For basic dissolution of iron or aluminum ($M$) in the presence of $Na_2O_2$:

$$Na_2O_2 = 2Na^+ + O_2^{2-} \quad , \tag{2}$$

$$K_2 = (a_{O_2^{2-}} \cdot a_{Na^+})/a_{Na_2O_2} \quad ,$$

$$M_2O_3 + 2O_2^{2-} = 2MO^{2-} + 5/2O_2 \quad , \tag{3}$$

$$K_3 = [(a_{MO_2^-})^2 \cdot p_{O_2}^{5/2}]/[a_{M_2O_3} \cdot (a_{O_2^{2-}})^2] \quad ,$$

where $K_i$ and $a_i$ represent equilibrium constants and chemical activities, respectively. Therefore, as $Na_2O_2$ is added to the melt, $a_{O_2^{2-}}$ increases (reaction 2), and, based on the dissolution reaction equilibrium represented by $K_3$, the concentration of $MO^{2-}$ in the salt (solubility) must increase. Alternatively, or additionally, the increased basicity due to the introduction of the peroxide can change the stable species (for example, $Fe_2O_3$ to $NaFeO_2$) and lead to increased

dissolution and/or growth of a product that is less mechanically compatible with the base material (causing delamination). The observation that pure $NaNO_3$ is more corrosive than the mixed $(Na,K)NO_3$ salt (see Fig. 6 and ref. 17) is consistent with a reaction process involving the formation of a sodium-containing product. The decreasing weight losses with increasing aluminum concentration of iron aluminide (see Table 3 and Fig. 9) tend to indicate that the $Fe_2O_3$ is more soluble or less mechanically compatible than $Al_2O_3$ over the basicity range of the subject experiments. The transitory effect of the peroxide additions (i.e., the higher corrosion rate is maintained only if $Na_2O_2$ is refreshed) indicates that the additions are consumed in the corrosion process and that they directly participate in, rather than simply accelerate, the corrosion reaction. Quantitative predictions of these effects depend on the generation of solubility data as a function of the activity of the oxide ion and, consequently, the development of a reference electrode for measuring basicity ($a_{O_2^{2-}}$) for this temperature range and salt, all of which is beyond the scope of the present study.

With the exception of zirconium and hafnium, all other refractory metals and alloys examined in this study exhibited weight changes indicative of severe to catastrophic corrosion. In many cases, this presumably resulted from rapid-oxidation kinetics and subsequent loss of the oxide product by dissolution or detachment. The extremely large standard deviations for such materials (see Tables 2 and 3) associated with the weight-change data reflect the variability associated with oxide formation and subsequent loss of the product layer during exposure or handling. The high corrosion rate of cobalt was probably a result of rapid oxidation accompanied by a loss of integrity because its oxide should have relatively low solubility in a basic solution.[21] The relatively good resistance of zirconium was reflected in net weight gains of the same order as the weight losses of NiAl (see Fig. 3). These weight gains are indicative of the formation of a stable, adherent oxide scale[17] and are consistent with weight gain measurements for exposed bulk $ZrO_2$. The observation that $ZrO_2$ gained a small, but significant, amount of weight when exposed to the salt would indicate

that a zirconate is a stable species and probably formed as the outer layer on zirconium (see Figs. 22 and 23). This would then explain the larger weight gain of zirconium (uptake of sodium and oxygen) compared to $ZrO_2$ (sodium only). As shown in Fig. 24, the weight gains appeared to be quite accurate measurements of the total depth of reaction layers on zirconium despite inaccuracies in determinations of reaction zone thickness because of cracking of the scale and inner zone. Although the cracking became more extensive as the exposure time (and scale thickness) increased (see Fig. 25), no extensive loss of scale was noted for up to 760 h of exposure. However, the growth kinetics of the reaction layers, even under the less aggressive open crucible conditions (see Fig. 26), and the significant solubility of oxygen in zirconium make long-term use of this metal in nitrate salt problematic, particularly in view of the greater propensity of scale cracking as the exposure time was increased (Fig. 25). In contrast, the thinner oxide product on hafnium and correspondingly smaller weight gain indicate potentially excellent resistance of this metal in aggressive nitrate salt systems, as also noted elsewhere.[17]

As shown in Table 4, high-density, high-purity ceramics (MgO, $Al_2O_3$, $ZrO_2$) yielded good weight change results. Of these, MgO appeared to be the most corrosion resistant (based on weight change only). As discussed above, the data showing weight losses for $Al_2O_3$ and gains for $ZrO_2$ are consistent with the results for zirconium and alloys containing significant amounts of aluminum, respectively. The presence of SiC whiskers in the alumina (for toughening) detrimentally affected the corrosion resistance in the nitrate salt (Table 4). This was expected due to the reactivity of this salt with silicon, but it is interesting to speculate whether corrosion resistance will increase to match that of pure alumina after the SiC has been preferentially removed from the near surface region. (This is somewhat doubtful in view of the high weight losses.) Such toughening of the bulk may be needed: the alumina crucibles used in the current investigation often cracked on cooling after containing the nitrate salt melt for extended periods of time (although they are not made from the advanced alumina used as the specimen material).

After considering the above gravimetric and microstructural data and other results,[17] it can be concluded that weight change is an adequate indicator of materials ranking for the aggressive nitrate salt environment of this study when all the possible components of such are evaluated. The most resistant materials to the salt mixtures used in these studies are hafnium (Table 3) and high-density MgO (Table 4), although neither can be considered practical for widespread applications. Hafnium is too expensive for uses where large quantities and economical operation are required, and MgO is not practical for the required piping systems. The same fabricability limitations are of concern for the other ceramics, although significant advances have been made recently in developing alumina and zirconia that can be used in somewhat complex geometries. However, in view of the potential fabricability and toughness problems with ceramics, higher aluminum-containing iron aluminides may offer promise for use in the aggressive nitrate-peroxide environment of the MOLTOX process because of their low raw material cost and relatively good corrosion resistance. Most standard alloys had (extrapolated) linear corrosion rates that were much too high (10-100 mm/year at 650°C) for MOLTOX applications. However, the rate for Fe-35 at. % Al in salt composition in the presence of peroxide (linear kinetics, see Figs. 5 and 8) was on the order of 1 mm/year, which may be within the range that can be accommodated by other system controls.[17]

In pure $NaNO_3$-$KNO_3$ at 650°C, iron aluminides should provide excellent corrosion resistance over long time periods because their corrosion rates decrease significantly with time (Fig. 5). As such, these materials could be improvements over Fe-Ni-Cr alloys even in the absence of $Na_2O_2$ since these latter materials showed significantly increased corrosion rates when exposure temperatures approached 650°C.[6,9] As shown in Fig. 9, an aluminum concentration of approximately 35 at. % is needed to minimize weight losses in nitrate salts with $Na_2O_2$. While higher aluminum concentrations might be of benefit for higher temperature, more aggressive salt conditions, they may severely limit ductility and fabricability. Another approach to improved corrosion behavior would be to use a highly protective,

compliant coating on a substrate material of moderate corrosion resistance and acceptable ductility (such as $Fe_3Al$). However, as shown in the current study (for other materials), commercial aluminizing did not improve protection in the molten nitrate salt because cracking of the aluminum-rich surface layer allowed ingress of the salt and exposure of the underlying metal (see Fig. 18). Conventional plasma spraying yielded a coating (zirconate) that was too porous to impart enhanced corrosion resistance.

The ongoing corrosion effort is part of the current development of corrosion-resistant iron aluminides with aluminum concentrations greater than 30 at. % and involves examination of the effects of other compositional and thermomechanical variations being used to produce ductile and fabricable alloys with adequate strength. This work also includes determination of the influences of microstructure and surface condition on corrosion resistance. Salt analyses will be used to better understand the relative contributions of iron, aluminum, and other alloy additions to the measured weight losses so as to provide timely input to the alloy design effort. Ultimately, as scale-up to larger heats of optimized-iron aluminide begins, effects of melting practices and fabrication processes on corrosion by the nitrate salt will be evaluated.

## SUMMARY

Investigations of the corrosion of various metals, alloys, and ceramics in high-temperature nitrate salt melts revealed that relatively few materials have acceptable compatibility in a 650°C $NaNO_3(-KNO_3)-Na_2O_2$ environment characteristic of the energy-saving MOLTOX chemical air separation process. Corrosion in these systems was controlled by the stabilities of the salt and solid-state surface oxides (whether they were pre-existing or formed upon exposure), the salt's oxide ion activity (strongly influenced by $Na_2O_2$ additions), and the physical condition of the solid surfaces. Weight changes and microstructural analyses of exposed specimens were used to identify the principal corrosion reactions and select the most promising materials for applications in this nitrate salt. In general, refractory/reactive

metals and alloys (with the exception of zirconium and hafnium), cobalt, nickel, Ni-Mo, TiAl, austenitic stainless steel, and Ni-Cr-Fe alloys were found to corrode quite readily because of rapid oxidation and/or dissolution in the salt. $Ni_3Al$ had a more moderate corrosion rate, while NiAl and iron aluminides with greater than about 35 at. % Al performed relatively well. Zirconium formed an apparently adherent corrosion product, but its scaling kinetics were such that long-term exposure to the salt is problematical. Hafnium appeared to be the most corrosion-resistant metallic material. High-density, advanced forms of $Al_2O_3$, $ZrO_2$, and MgO were quite stable in the salt. More porous ceramics did not perform well because of salt uptake and mechanical crumbling. A similar degradation phenomenon was observed for plasma-sprayed zirconate coatings on nickel aluminides. Analysis of specimens exposed in the APCI MOLTOX pilot plant showed that commercially aluminized coatings did not impart any increased protection to the substrate materials due to extensive cracking of the high-aluminum surface layers.

Microstructural analysis of aluminized and aluminide specimens exposed to the nitrate salt revealed some evidence of $NaAlO_2$, which is thermodynamically stable in the nitrate salt environment, but there was no direct observation that this product adhered to the exposed material. However, the formation of $NaAlO_2$ and a thin $Al_2O_3$ surface layer apparently controlled the corrosion process such that the reaction rates of iron aluminides were significantly better than most other candidate alloys. The presence of $Na_2O_2$ in the nitrate exacerbated the corrosion of aluminides due to an increase in the basicity of the salt, but, for a fixed concentration, its influence decreased with time. Weight-loss kinetics were approximately linear for Fe-35 at. % Al when the $Na_2O_2$ content of the salt was periodically refreshed (which more closely simulates the MOLTOX condition). The investigation of the corrosion of iron aluminides is continuing with emphasis on providing appropriate input into the alloy development process.

## REFERENCES


1. R. W. Carling and R. W. Mar, *Industrial Use of Molten Nitrate/Nitrite Salts*, SAND81-8020, Sandia National Laboratories, Albuquerque, NM, December 1981.

2. R. W. Mar and R. W. Carling, "The Application of Molten Salts to Solar Large Power Systems," pp. 473-484 in *Proc. Third Int'l. Symp. Molten Salts,* (eds. G. Mamantov, M. Blander, and G. P. Smith, Vol. 81-9, The Electrochemical Society, Princeton, NJ, 1981.

3. B. R. Dunbobbin and W. R. Brown, *Pilot Plant Development of a Chemical Air Separation Process*, DOE/CE/40544-1, U.S. Department of Energy, February 1987.

4. R. W. Bradshaw, *Corrosion of 304SS by Molten $NaNO_3$-$KNO_3$ in a Thermal Convection Loop*, SAND80-8856, Sandia National Laboratories, Albuquerque, NM, December 1980.

5. R. W. Bradshaw, *Thermal Convection Loop Corrosion Tests of 316 and IN800 in Molten Nitrate Salts*, SAND81-8210, Sandia National Laboratories, Albuquerque, NM, February 1982.

6. R. W. Bradshaw, *Oxidation and Chromium Depletion of Alloy 800 and 316SS by Molten $NaNO_3$-$KNO_3$ at Temperatures Above 600°C*, SAND86-9009, Sandia National Laboratories, Albuquerque, NM, January 1987.

7. R. W. Bradshaw, "Thermal Convection Loop Study of the Corrosion of Incoloy 800 in Molten $NaNO_3$-$KNO_3$," *Corrosion* **43**, 173–78 (1987).

8. R. W. Bradshaw, *A Review of the Chemical and Physical Properties of Molten Alkali Nitrate Salts and Their Effect on Materials Used for Solar Central Receivers*, SAND87-8005, Sandia National Laboratories, Albuquerque, NM, April 1987.

9. P. F. Tortorelli and J. H. DeVan, *Thermal Convection Loop Study of the Corrosion Of Fe-Ni-Cr Alloys by Molten $NaNO_3$-$KNO_3$*, ORNL/TM-8298, Oak Ridge National Laboratory, Oak Ridge, TN, December 1982.

10. A. J. Arvía, J. J. Podestá, and R. C. V. Piatti, "Kinetics of Iron Passivation and Corrosion in Molten Alkali Nitrates," *Electrochem. Acta* **17**, 33–44 (1972).

11. N. Ramasubramanian, "Potential/$pO^{2-}$ Diagrams and Passivation of Iron in Molten Alkali Nitrates," pp. 215-227 in *Proc. Equilibrium Diagrams: Localized Corrosion*, Vol. 84-9, The Electrochemical Society, Princeton, NJ, 1984.

12. P. Spiteri et al., "Etude de la Corrosion de Différents Aciers par le Mélange Fondu de Nitrate-Nitrie Alcalins," *Mater. Sci. Eng.* **87**, 369-78 (1987).

13. A. Baraka, A. I. Abdel-Rohman, and A. A. El Hosary, "Corrosion of Mild Steel in Molten Sodium Nitrate-Potassium Nitrate Eutectic," *Br. Corrosion J.* **11**, 44–46 (1976).

14. A. A. El Hosary, A. Baraka, and A. I. Abdel-Rohman, "Effect of Acid and Base Additions on the Corrosion of Mild Steel in Molten $NaNO_3$-$KNO_3$ Eutectic," *Br. Corrosion J.* **11**, 163-67 (1976).

15. A. Baraka, R. M. S. Baraka, and A. Abdel-Razik, "The Corrosion Behaviour of Nickel in Molten $NaNO_3$-$KNO_3$ Eutectic," *Surf. Technol.* **26**, 199-206 (1985).

16. G. S. Picard, H. M. Lefebvre, and B. L. Trémillon, "Thermodynamic Study of Corrosion of Iron in $NaNO_3$-$NaNO_2$ Mixtures," *J. Electrochem. Soc.* **134**, 52-58 (1987).

17. *APCI Corrosion Studies In Support of MOLTOX™*, to be published as DOE/CE report, U.S. Department of Energy.

18. S. Taniguchi, T. Shibata, and H. Tsuruoka, "Isothermal Behavior of $Ni_3Al$-0.1B Base Alloys Containing Ti, Zr, or Hf Additions," *Oxid. Met.* **26**, 1–17 (1986).

19. J. H. DeVan, "Mechanical Properties of Oxide Films and Correlation With Metal/Oxide Interface," pp. 48-54 in *Fossil Energy Program Semiannual Progress Report for October 1986 Through March 1987*, ORNL-6395, Oak Ridge National Laboratory, Oak Ridge, TN, August 1987.

20. H. S. Hsu, *Corrosion of Fe-25Cr-20Ni Alloy in Molten Alkali Carbonates*, ORNL-6354, Oak Ridge National Laboratory, Oak Ridge, TN, March 1987.

21. R. A. Rapp, "Chemistry and Electrochemistry of Hot Corrosion of Metals," *Mater. Sci. Eng.* **87**, 319–27 (1987).

22. D. Kang, Air Products and Chemicals, Inc., private communication, to P. F. Tortorelli, Oak Ridge National Laboratory, April 1989.

## INTERNAL DISTRIBUTION

1-2. Central Research Library
3. Document Reference Section
4-5. Laboratory Records Department
6. Laboratory Records, ORNL RC
7. ORNL Patent Section
8-10. M&C Records Office
11. P. Angelini
12. T. M. Besmann
13-17. P. S. Bishop
18. W. D. Bond
19. R. A. Bradley
20. R. S. Carlsmith
21. P. T. Carlson
22. L. G. Christophorou
23. D. F. Craig
24-28. J. R. DiStefano
29. R. R. Judkins
30-34. M. A. Karnitz
35. J. R. Keiser
36. C. T. Liu
37. E. L. Long, Jr.
38. C. G. McKamey
39. W. D. Porter
40. A. C. Schaffhauser
41. M. A. Schmidt
42. G. M. Slaughter
43. V. J. Tennery
44-48. P. F. Tortorelli
49. D. F. Wilson
50. A. D. Brailsford (Consultant)
51. H. D. Brody (Consultant)
52. F. F. Lange (Consultant)
53. D. P. Pope (Consultant)
54. E. R. Thompson (Consultant)
55. J. B. Wachtman, Jr. (Consultant)

## EXTERNAL DISTRIBUTION

56. W. R. Brown
Air Products and
Chemicals, Inc.
P.O. Box 538
Allentown, PA 18105

57. B. R. Dunbobbin
Air Products and
Chemicals, Inc.
P.O. Box 538
Allentown, PA 18105

58. E. Givens
Air Products and
Chemicals, Inc.
P.O. Box 538
Allentown, PA 18105

59. A. J. Heckler
Manager, New Materials
Armco, Inc.
703 Curtis Street
Middletown, OH 45043

60. G. L. Houze, Jr.
Director, Research and
Analytical Laboratories
Allegheny Ludlum Corporation
Technical Center
Alabama & Pacific Avenues
Brackenridge, PA 15014-1597

61. D. Kang
Air Products and
Chemicals, Inc.
P.O. Box 538
Allentown, PA 18105

62. P. W. Lee
Research Scientist
The Timken Company
1835 Dueber Avenue, SW
Canton, OH 44706

63. R. McDonald
President
Metallamics
P.O. Box 1539
Traverse City, MI 49685-1539

64. A. Neupaver
Ametek Operations Headquarters
Specialty Metals Division
Route 519
84, PA 15330

65. J. W. Slusser
Air Products and
Chemicals, Inc.
P.O. Box 538
Allentown, PA 18105

66. Ellis D. Vevink, Jr.
Department of Materials
Science and
Engineering
University of Florida
Gainesville, FL 32611

67. Assistant Manager for
Energy Research and
Development
Department of Energy
Oak Ridge Operations
Office
P.O. Box 2001
Oak Ridge, TN 37831-8600

68-77. Department of Energy
Office of Scientific and
Technical Information
Office of Information
Services
P.O. Box 62
Oak Ridge, TN 37831

For distribution by
microfiche as shown in
DOE/OSTI-4500,
Distribution Categories
UC-311 (Separation
Technology Research) and
UC-368 (Corrosion Resistant
Materials).